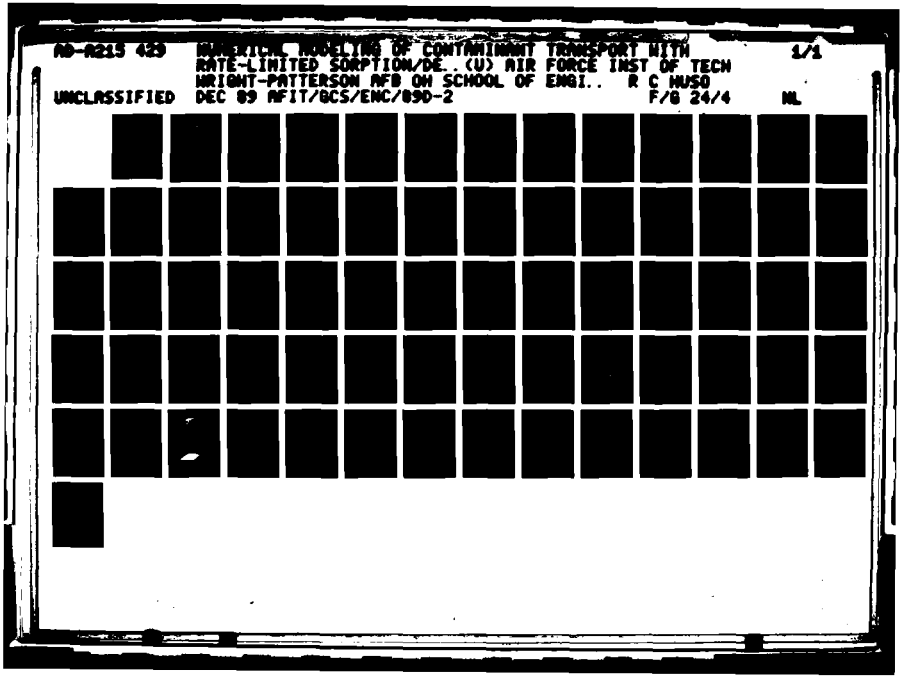
AD-A215 429
NUMERICAL MODELING OF CONTAMINANT TRANSPORT WITH RATE-LIMITED SORPTION/DE..(U) AIR FORCE INST OF TECH WRIGHT-PATTERSON AFB OH SCHOOL OF ENGI.. R C MUSO
1/1
UNCLASSIFIED
DEC 89 AFIT/GCS/ENC/89D-2
F/G 24/4
NL

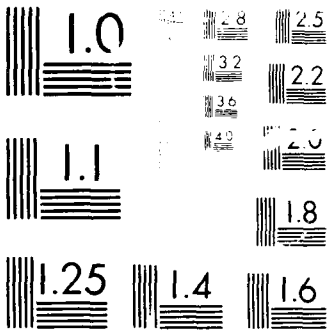
1.0
1.1
1.25
1.4
1.6
1.8
2.2
2.5
3.2
3.6
4.0

(1)

NUMERICAL MODELING OF CONTAMINANT TRANSPORT WITH RATE-LIMITED SORPTION/DESORPTION IN AN AQUIFER

THESIS

Rand C. Huso
Captain, USAF

AFIT/GCS/ENC/89D-2

DEPARTMENT OF THE AIR FORCE
AIR UNIVERSITY
AIR FORCE INSTITUTE OF TECHNOLOGY

Wright-Patterson Air Force Base, Ohio

AFIT/GCS/ENC/89D-2

NUMERICAL MODELING OF CONTAMINANT TRANSPORT WITH RATE-LIMITED SORPTION/DESORPTION IN AN AQUIFER

THESIS

Rand C. Huso
Captain, USAF

AFIT/GCS/ENC/89D-2

AFIT/GCS/ENC/89D-2

NUMERICAL MODELING OF CONTAMINANT TRANSPORT WITH RATE-LIMITED SORPTION/DESORPTION IN AN AQUIFER

THESIS

Presented to the Faculty of the School of Engineering

of the Air Force Institute of Technology

Air University

In Partial Fulfillment of the

Requirements for the Degree of

Master of Science (Computer Systems)

Rand C. Huso, B.S.

Captain, USAF

December 1989

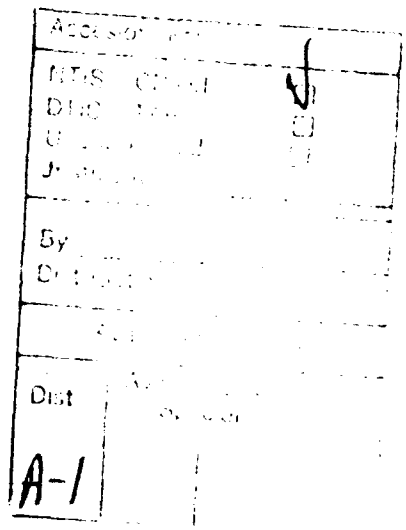

Approved for public release; distribution unlimited

Acknowledgments

I am grateful to many whose support provided me the privilege of writing and receiving credit for this thesis. For assistance with the overall stability analysis I'm indebted to my thesis advisor, Dr. Mark Oxley. I thank Mark also for his enthusiasm and the countless hours he spent listening to all the problems I encountered.

Thanks to Dr. Dave Umphress for giving me a desk and access to the Sun Workstation for writing this thesis and for the opportunity to teach two classes. I quite enjoyed them.

For assistance with the equation set and lots of help locating articles, I thank Dr. Mark Goltz, and for the funds to attend a training class in groundwater modeling.

For moral support, I am indebted to many as well. I thank my wife Marcía for sticking by me with endless patience as I labored deep into the night and kept hours only the nocturnal creatures would understand. A big thanks to my children Kai Bjørn and Brynn Andrea:

THE KID

Thou little Kid didst play

&c (4:153)

And thanks to the Almighty for an incredibly beautiful planet. May this and similar research help to restore the pristine primitiveness the planet once knew.

Rand C. Huso

Table of Contents

List of Figures

List of Tables

Abstract

This paper traces the development of the understanding of contaminant transport in an aquifer for a radially symmetric region. It presents the progression of ideas and equations leading to the equation set describing the advective/dispersive mechanisms coupled with rate-limited adsorption. This equation set is converted to a numerical scheme in the Fortran language using finite elements and finite differences. The resulting model is tested against the Laplace transform solution to the same equation set, and several graphs are presented detailing the comparison.

NUMERICAL MODELING OF CONTAMINANT TRANSPORT WITH RATE-LIMITED SORPTION/DESORPTION IN AN AQUIFER

I. Introduction

1.1 Theme and Goals

Years of accidental or deliberate dumping of petroleum products and hazardous waste materials has resulted in polluted groundwater. The Department of Defense is engaged in a massive program, known as the Installation Restoration Program, to cleanup these polluted environments on military installations, and the Environmental Protection Agency is funding research to help in the cleanup efforts. These cleanup efforts often involve drilling wells in the vicinity of the contaminated area and evacuating water until the concentration of pollutant is reasonably low (9:1329), (19), (22:630).

The planners at these remediation sites use tools to estimate how long the wells must operate based on some initial sample data and sound judgment. These tools are frequently numerical simulations of the advective/dispersive transport equation that are fine-tuned for each type of pollutant and aquifer geometry. To assist the modelers, studies have been conducted in laboratories to determine the fate of pollutants in various soils (33, 5). Many recent efforts attempt to compare various mathematical models to laboratory data and field data (6, 21, 18, 30, 16, 35, 15), or even to simulated data (37, 9). These investigations assess the impact of adsorption of organic pollutants in different types of soil. This information is used to upgrade the accuracy of the models and to adjust the methods employed in the models and the remediation efforts.

The numerical modeling of contaminant transport in polluted groundwater is an important part of the remediation. The knowledge gained by running these models can be used by planners to make predictions about the cost and duration of cleanup efforts, and to gain further understanding

of the physical processes involved in the transport of foreign materials in the aquifer itself. The advection/dispersion equation has traditionally been used to model the transport of contaminants. It uses a retardation factor to account for the chemical sorbing to the aquifer materials, implying the local equilibrium assumption (LEA), where equilibration between sorbed and aqueous phases occurs instantly (2).

With this thesis I propose a numerical solution of the mathematical model of the standard transport equation (2) modified to incorporate diffusion into and out of regions with immobile water. These regions of immobile water may contribute to rate-limited sorption/desorption of contaminant, and have a significant impact on aquifer remediation. Sand and gravel aquifers are the only ones considered in this research, and the unsaturated zone is ignored (the unsaturated zone is the zone just above the water table). The main items of interest in this effort are the modeling of the breakthrough curve as the contaminant is pumped out of the aquifer, the retardation of the contaminant due to sorption, the contribution of the immobile zone diffusion to the 'tailing' of the breakthrough curve, and the effect of pulse pumping (variation in the pumping rate) on remediation.

The concentrations in the water extracted from a well during pump-and-treat remediation is governed, in part, by the transfer of the chemicals from a reservoir of contaminant (sorbed or otherwise) to the flowing water (22:632).

The goals of this research are:

1. Create a numerical model that can be run on a small computer. The model will be based on the transport equation and will include the physics of rate-limited sorption/desorption in a heterogeneous aquifer.
2. Using the model, demonstrate the breakthrough curve and the observed tailing for suitable choices of the input parameters. This will partially validate the numerical solution of the diffusion-limited transport mechanism, and give insight into the effect of rate-limited adsorption on the fate of these pollutants.
3. Demonstrate how a variation in the pumping rate (pulse pumping) might be used advantageously by those involved in the remediation, and how slow desorption will effect the contaminant concentrations after the pumping stops.
4. Gain a practical understanding of finite difference and finite element methods used in modeling.

1.2 Background

The simplest contaminant transport model incorporates advection, dispersion, and equilibrium sorption to simulate the movement of a pollutant in an aquifer. This simple model may be suitable when relatively low levels of contamination are not of significance. However, when very low levels of contamination are significant, such as during remediation of an aquifer contaminated with an organic pollutant, the simple advective/dispersive model is insufficient for demonstrating the tailing that has been found in field and in laboratory experiments (19). One explanation for this tailing (whereas the advective/dispersive model predicts a virtually symmetric breakthrough curve) is the existence of areas in the aquifer where the water doesn't flow. The contaminants diffuse into these immobile regions due to the existence of a concentration gradient. This is further exacerbated by there typically being a larger porosity in these low permeability immobile zones (22:634). As the well pumps, and the main mass of pollutant is advected away, the gradient changes and the chemicals begin to diffuse out of these immobile zones back into the moving water (the mobile region). As the chemicals diffuse out of these immobile regions, the resultant flux produces only a slow decrease in the level of contaminant extracted from the well, or experienced in the laboratory (the tailing).

Coats and Smith proposed a mathematical model to account for this phenomenon. They postulated the existences of immobile zones due to dead end pores (10). In their model, the contaminant moves between the mobile and immobile regions at a rate proportional to the gradient of the concentrations in the two regions. Their method was avoided for many years because of computational difficulties (21:276).

1.3 Statement of the Problem

Goltz (14) (13) presented an analytical model which includes Fickian diffusion in immobile zones. It uses diffusive exchange between the two regions (mobile zone and immobile zone) and uses the advective/dispersive equation to model transport in the mobile region, thus allowing for the slow sorption and desorption of contaminant between mobile and immobile zones. This mathematical model assumes axial symmetry of the contaminant from an extraction well out to some arbitrary

distance. The initial contaminant concentration from the well out is assumed constant, dropping to zero at the border of the contaminated region. A model that allows for more general boundary and initial conditions is one step toward a model that may be used by planners at a cleanup site.

1.4 Scope of the Research

This research details the creation of a numerical model based on the physical principle of mobile and immobile zones with the possibility of Fickian diffusion in the immobile zone. The numerical model will be compared with the analytic solution of Goltz (13) to confirm the correctness of the model.

1.5 Assumptions

There are several assumptions in the formulation of the model:

- With any flow rate there will be a drawdown (see Figure 1.1). In the model, drawdown of

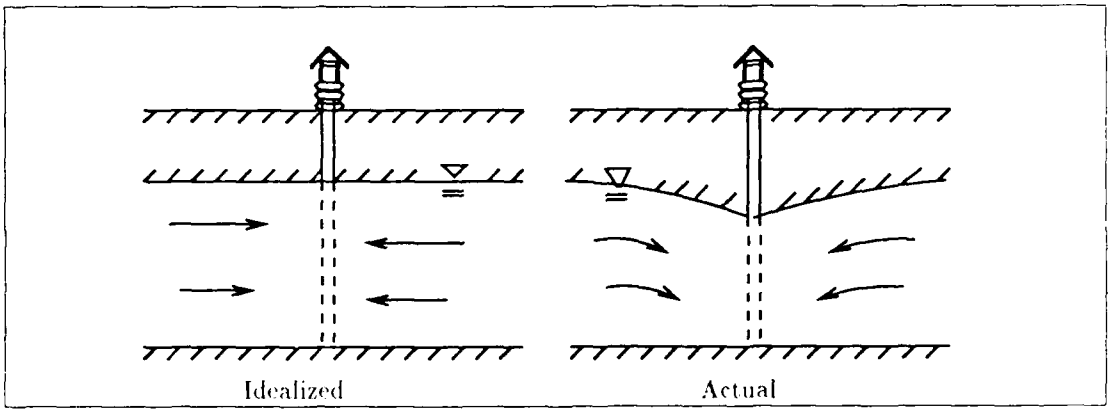

Figure 1.1. Drawdown assumption around a fully penetrating well in an aquifer

the height of the aquifer due to the pumping is ignored.

- The model assumes a homogeneous aquifer material.
- The height of the aquifer is constant, the flow is not fractal, and the background seepage rate is negligible when compared with the water movement due to pumping.

- The contamination has a radial symmetry and is throughout the vertical extent in the aquifer (see Figure 1.2). In reality the concentration distribution would depend upon how the aquifer

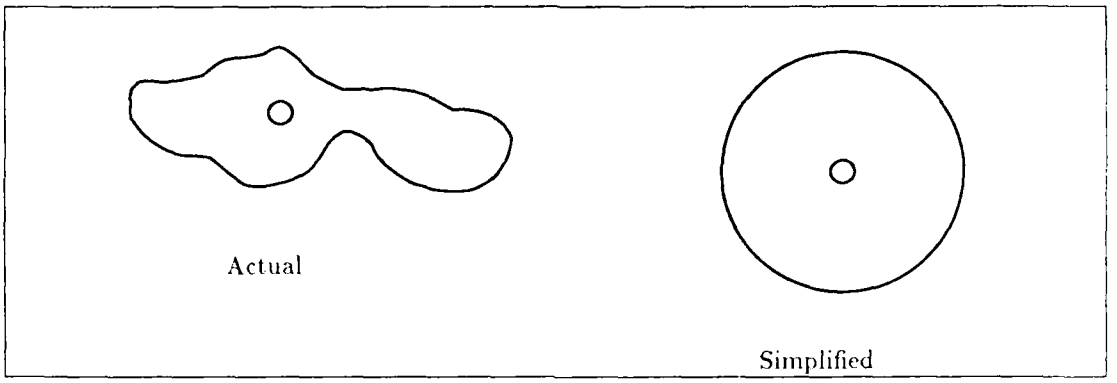

Figure 1.2. Radial Symmetry of contaminant profile versus Reality

was contaminated. It is also assumed that the concentration is limited, and no further contamination takes place i.e., no external sources or sinks of pollutant.

- The molecular diffusion in the mobile region is much smaller than the dispersion caused by the velocity induced by the pump (33).

1.6 Materials and Support Requirements

Successful completion of the goals of this thesis required the availability of user-friendly computer hardware and a standardized computer language accepted by the scientific community. Both the Sun workstation and various high-end personal computers were considered as candidate hardware systems. The Fortran language was the obvious choice for this scientific application because of the availability of optimized compilers and numerous well-tested numerical recipes (27). The Sun workstation was readily available and had the necessary compiler and graphics utility (Mathematica), but lacked the IMSL routines. I chose the Amiga over the other available high-end personal computers because of its system-level multitasking, reasonable price, speed, and color graphics. I chose the Absoft AC/FORTRAN compiler (1) because it implements the entire ANSI X-3.9 1978 standard (commonly known as Fortran-77) (23). As it happened, the Absoft compiler compiled the source code considerably faster on the Amiga than the compiler on the Sun 3/50!

1.7 Overview

The overall thesis effort consisted of four key phases. We begin with a survey of recent literature in the field of modeling sorption processes during contaminant transport, and develop the mathematical expressions implemented in the numerical model. Then we develop the numerical schemes used to transform the system of partial differential equations into a form suitable for programming on a computer, and briefly examine the numerical properties of stability, consistency, and convergence for the numerical methods. And finally, we present the results of sample executions, and compare them with the computer-based analytical solutions of Goltz (13).

The main part of the thesis is presented here, with the source code available as an appendix from the Mathematics and Computer Science Department of the Air Force Institute of Technology.

II. Mathematical Formulation of the Problem

2.1 Introduction

Cleanup procedures at sites where toxic materials have contaminated the groundwater often include pumping the contaminated water out of the aquifer until the level of contamination is acceptable (9:1329). The models presently in use to help in the aquifer cleanup efforts do not account for the possibility of rate-limited sorption/desorption and molecular diffusion in regions of low permeability (13, 22). Due to rate-limited desorption, the toxic materials may persist longer and at a much higher concentration than predicted by models which assume equilibrium sorption/desorption.

The following sections examine the efforts of researchers to develop a mathematical model to account for more of the known physical processes in contaminant transport. These mathematical models necessarily precede the development of computer based solutions.

2.2 The Advective/Dispersive Model and Linear Sorption

The traditional way to model contaminant transport is with advection, dispersion, and some exchange of contaminant with the solid material in the aquifer. Equation 2.1 shows, in cylindrical coordinates, the mass balance typically used to account for these processes.

$$\frac{\partial C}{\partial t} + \frac{\rho}{\theta}\frac{\partial S}{\partial t} = \frac{1}{r}\frac{\partial}{\partial r}\left[r\ D\ \frac{\partial C}{\partial r}\right] - V(r)\ \frac{\partial C}{\partial r} \tag{2.1}$$

where

$C(r,t)$ = contaminant concentration in the mobile zone [M/L^3]
r = radial coordinate [L]
t = time [T]
$S(r,t)$ = sorbed contaminant [unitless]
$V(r)$ = seepage velocity [L/T]
ρ = bulk density of aquifer material [M/L^3]
θ = aquifer porosity [unitless]

The term $D = A_l|V(r)| + D^*$ is the hydrodynamic dispersion coefficient $[L^2/T]$. A_l is the longitudinal dispersivity of the porous medium $[L]$, $|V(r)|$ is the magnitude of the seepage velocity $[L/T]$, and D^* is the molecular diffusion coefficient $[L^2/T]$. The seepage velocity is given by

$$V(r) = \frac{-Q_w}{2\pi\ r\ H\ \theta} \tag{2.2}$$

where Q_w is the pumping rate at the well $[L^3/T]$, H is the mean height of the aquifer $[L]$, and θ is the porosity or volumetric moisture content of the aquifer [unitless].

The molecular diffusion is usually taken to be very small compared to the dispersion, and the D^* term is dropped. This is certainly true near the well when the well is pumping, but becomes less accurate as we get further from the well, or as the flow rate at the well decreases.

The many models currently in existence differ primarily on how the $\frac{\partial S}{\partial t}$ term is represented (6:34) . Nonlinear sorption isotherms are typically represented with the Freundlich equation: $S = K_d\ C^n$ (6)[35]. The standard procedure assumes equilibrium and a linearity between the time rates of change of the sorbed and aqueous solvent, viz., $S = K_d\ C$, where K_d is the distribution coefficient $[L^3/M]$ and $n = 1$. Substituting this into Equation 2.1 produces:

$$R\ \frac{\partial C(r,t)}{\partial t} = \frac{1}{r}\frac{\partial}{\partial r}\left[r\ D\ \frac{\partial C(r,t)}{\partial r}\right] - V(r)\ \frac{\partial C(r,t)}{\partial r} \tag{2.3}$$

Where $R = 1 + \frac{\rho K_d}{\theta}$ is the retardation factor [unitless]. This will account for some retarding of the pollutant as it temporarily adheres to the materials in the aquifer. This is known as the local equilibrium assumption (or LEA) (3).

2.3 Sorption Kinetics

One of the very early attempts to mathematically model diffusion processes in adsorption columns is that by Lapidus and Amundson (20). In their 1952 paper they propose a diffusion process as the cause of slight deviations between predictions and laboratory results.

The asymmetry in the effluent concentration profiles from laboratory experiments with columns of soil led Coats and Smith (10) to postulate the existence of immobile zones within the aquifer material. They proposed a differential capacitance mathematical model equivalent to

that of Lapidus and Amundson, with diffusion into small stagnant volumes of water. Their equation set in one spatial dimension is given here (10:76):

$$\lambda\frac{\partial C}{\partial t} + (1-\lambda)\frac{\partial S}{\partial t} = D\frac{\partial^2 C}{\partial x^2} - V\frac{\partial C}{\partial x} \quad \text{mobile region} \tag{2.4}$$

$$(1-\lambda)\frac{\partial S}{\partial t} = K(C-S) \quad \text{immobile region} \tag{2.5}$$

Where S is the concentration in the stagnant volume $[M/L^3]$, C is the concentration in the mobile region, λ is the fraction representation of stagnant to mobile [unitless], and K is the constant describing the rate of exchange between stagnant and mobile regions $[T^{-1}]$. Their results indicated the total mixing observed in laboratory experiments was the result of more than just the dispersion mechanism. (10:78)

Van Genuchten and Wierenga continue these ideas but allow for a sorbing contaminant (36:473). Using their notation, the following expression describes contaminant transport within the mobile region of an aquifer in cylindrical coordinates:

$$\frac{\partial C_m(r,t)}{\partial t} = \frac{A_l|V(r)|}{R_m}\frac{\partial^2 C_m(r,t)}{\partial r^2} - \frac{V(r)}{R_m}\frac{\partial C_m(r,t)}{\partial r} - \frac{\theta_{im}R_{im}}{\theta_m R_m}\frac{\partial C_{ima}(r,t)}{\partial t} \tag{2.6}$$

where $C_{ima}(r,t)$ is the average concentration in a representative volume of the immobile region $[M/L^3]$, A_l is the dispersivity $[L]$, θ_m and θ_{im} are the porosities of the mobile and immobile regions, respectively [unitless].

The effect of these immobile zones on the mobile contaminant concentrations is controlled by the ratios of the porosities of the two zones and the ratios of their retardation factors. The retardation factors are now

$$R_m = 1 + \frac{f\ \rho\ K_d}{\theta_m} \tag{2.7}$$

for the mobile zone [unitless] and

$$R_{im} = 1 + \frac{(1-f)\ \rho\ K_d}{\theta_{im}} \tag{2.8}$$

for the immobile zone [unitless]. The term f denotes the fraction of sorption sites in contact with mobile fluid [unitless].

Rao and others (29:684) measured diffusion in porous ceramic spheres for some chemicals that do not adsorb in an attempt to describe solute transport in aggregated porous media with distinct mobile and immobile zones. A Fickian diffusion model was used to fit the experimental data. The results pointed favorably toward a diffusion model to describe solute transfer between these porous spheres and the mobile region (29:687).

Nkedi-Kizza and others examined more breakthrough concentration curves from laboratory experiments to explain the tailing of both nonsorbing and sorbing pollutants (25:471). They coupled the standard advective/dispersive model presented earlier with Fick's second law of diffusion. Their calculations agreed favorably with measurements in the laboratory, verifying the utility of assuming diffusive solute transfer to describe transport in aggregated porous media (25:475).

Sudicky and others (32) put this model to the test in a laboratory experiment by creating an aquifer of thin sand sequestered by layers of silt. Their results indicated that the effect of molecular diffusion within the silt zones was more important than the dispersive effects in the mobile zone for understanding the fate of the contaminant. The longitudinal diffusion (dispersion) was of secondary importance.

Miller and Weber concentrated their effort on the rate-limited effects of diffusion by examining a variety of mathematical models for predicting contaminant fate and transport in the light of laboratory experiments. They concluded that the process of sorption in their systems was rate-limited, and the best fit was obtained by models that incorporated intraparticle diffusion (24:243,260).

The equation frequently used to describe Fickian diffusion within the immobile zone is

$$\frac{\partial C_{im}(r,z,t)}{\partial t} = \frac{D_e}{z^{\nu-1}R_{im}}\frac{\partial}{\partial z}\left[z^{\nu-1}\frac{\partial C_{im}(r,z,t)}{\partial z}\right] \tag{2.9}$$

where C_{im} is the concentration of the contaminant in the immobile zone.

The retardation factor R_{im} accounts for contaminant sorption within the immobile zone, and is called the immobile zone retardation factor. The diffusion coefficient in the immobile zone is D_e $[L^2/T]$. The term ν defines the type of immobile region geometry:

$\nu = 1$ for Layered Immobile Region Geometry
$\nu = 2$ for Cylindrical Immobile Region Geometry
$\nu = 3$ for Spherical Immobile Region Geometry

To couple this equation with the mobile region mass balance equation (Equation 2.6), volume averaging is used. The amount of contaminant entering/leaving the mobile region must equal the amount of contaminant leaving/entering the immobile region. The amount of contaminant in the immobile zone is given by

$$C_{ima}(r,t) = \frac{\nu}{b^{\nu}} \int_0^b z^{\nu-1} C_{im}(r,z,t) dz \tag{2.10}$$

where b is the halfwidth of a typical immobile zone [L], and ν defines the type of immobile region geometry. One of the findings of Nkedi-Kizza and others (25:475) was that a reasonable range of sizes and shapes of aggregates could be approximated by a representative spherical aggregate.

2.4 The Model Equation Set

The equation for the mass balance (Equation 2.6) needs the knowledge of what transpires in the immobile zones, to determine the last term on the right hand side of the equation.

The governing equation for the immobile zone depends upon whether ν is one, two, or three. For $\nu = 1$ Equation 2.9 becomes

$$\frac{\partial C_{im}(r,z,t)}{\partial t} = \frac{D_e}{R_{im}} \frac{\partial^2 C_{im}(r,z,t)}{\partial z^2} \tag{2.11}$$

and the volume averaging equation (Equation 2.10) becomes

$$C_{ima}(r,t) = \frac{1}{b} \int_0^b C_{im}(r,z,t)\, dz \tag{2.12}$$

These equations (2.6, 2.11, and 2.12) form a complete set describing advection and dispersion in a radially symmetric aquifer with immobile layers of clay or other layered sorbate (see Figure 2.1).

When $\nu = 3$ Equation 2.9 becomes

$$\frac{\partial C_{im}(r,z,t)}{\partial t} = \frac{D_e}{R_{im}} \left[\frac{\partial^2 C_{im}(r,z,t)}{\partial z^2} + \frac{2}{z} \frac{\partial C_{im}(r,z,t)}{\partial z} \right] \tag{2.13}$$

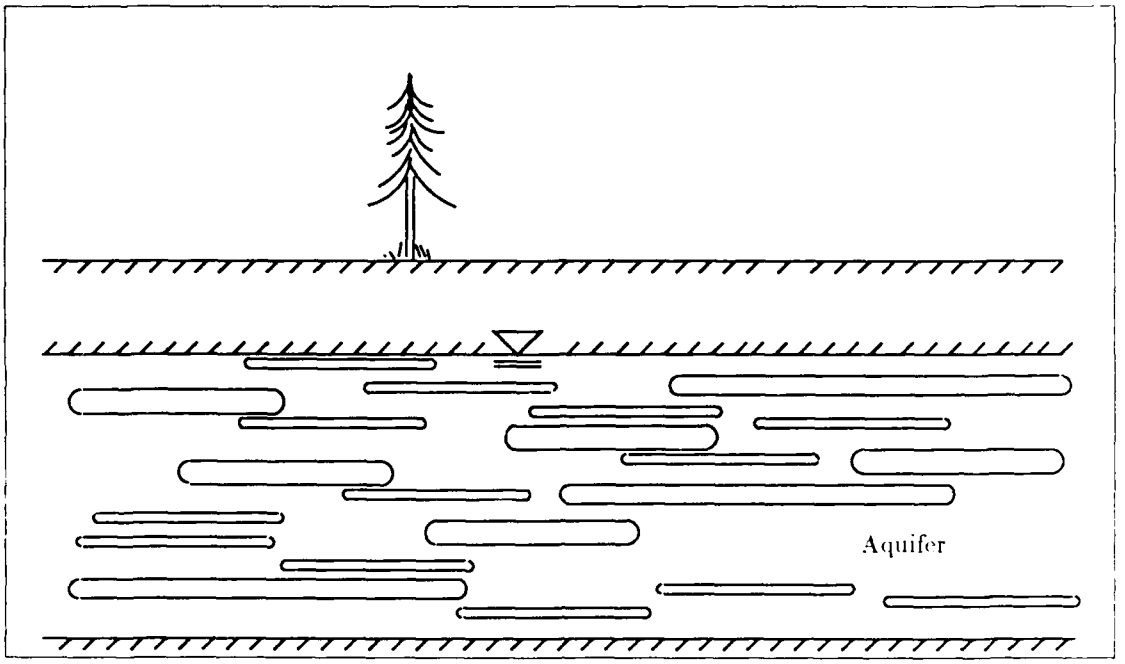

Figure 2.1. Layered Immobile Zones in an Aquifer

and Equation 2.10 becomes

$$C_{ima}(r,t) = \frac{3}{b^3} \int_0^b z^2 \, C_{im}(r,z,t) \, dz \tag{2.14}$$

These equations (2.6, 2.13, and 2.14) describe spherical immobile regions in the aquifer where the contaminant may undergo adsorption (see Figure 2.2).

These equations form the basis of the numerical model examined in the next chapter.

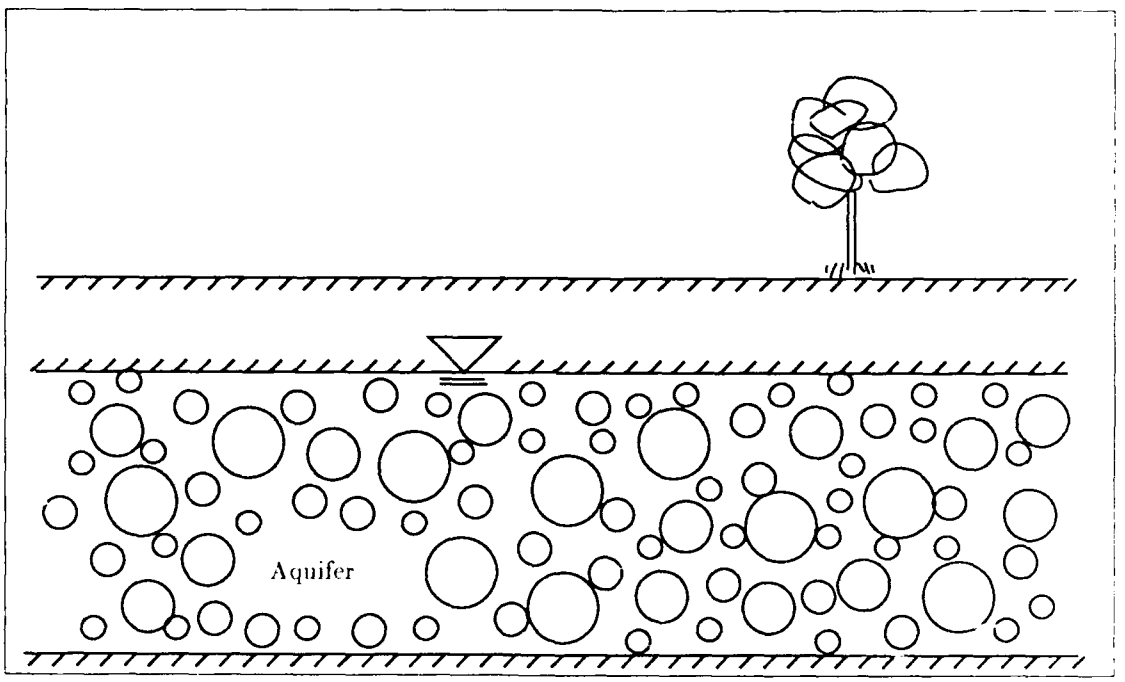

Figure 2.2. Spherical Immobile Zones in an Aquifer

III. Numerical Methods

3.1 Problem Statement

In the last chapter we looked at the theoretical and experimental evidence for including rate-limited sorption/desorption physics in our contaminant transport model. This chapter presents the numerical implementation of these equations. This implementation uses numerical quadrature techniques, the Finite Element Method (FEM) and Finite Difference Method (FDM) to transform the partial differential equations into an algorithm suitable for the Fortran language.

3.2 Program Design

Beginning with Equations 2.9, 2.10, and 2.6 as representing either the layered or spherical geometry, the preferred solution would be a transform that combines the two regions and these three equations into a single equation. The Laplace transform was attempted, but the restrictions of a formula representation of the levels of contaminant in both regions was unacceptable. With this restriction, the model could not simulate pulse pumping. These equations are solved for the special case of a constant level of the contaminant from the well center out an arbitrary distance and then down to zero (13). This Laplace transform solution will be discussed in Chapter 4.

The simplest and most obvious solution was to keep arrays of gridded data for each region. Figure 3.1 shows the representation implemented in this thesis. The mathematical formula for the seepage velocity in the mobile region presents a fictitious singularity at the well center. To overcome this problem, the grid begins a slight distance from the well center: an approximation to the boundary of the well itself. The grid for the immobile zone is more elaborate than that for the mobile zone because of the need to maintain a sufficient number of grid points to properly represent a gradient profile for the Fickian diffusion.

The model will step forward within the immobile region a small amount of time (solving Equation 2.9, and then integrate (solving Equation 2.10). These new values will then be used to calculate new values in the mobile zone by stepping forward in time using Equation 2.6. This process will be repeated until the final time is reached.

3.2.1 Data Flow Oriented Design In order to implement pulse pumping, the model needs the ability to stop the flow rate after a specified time and begin again with reduced or increased flow rates, and perhaps adjust other parameters like the duration of the simulated execution. Rather than have the model run interactively and solicit information periodically from the user, it will create an output file that contained the same information as the input file. With this design, the model could cycle on its own data, keeping the output contaminant levels for both regions, grid sizes, and other grid information from one execution and using this as input to the next run.

Because of the large number of input parameters, two input files were chosen: one for the parameters that were subject to change and 'tuning', and one for the grid and contaminant level information.

These files are shown in the data flow diagram (Figure 3.2) and the formats of these files are shown in the documentation header for the routines that read them (GPARMS and GETHCM).

3.2.2 Transform/Transaction Analysis Transform analysis was chosen as an overall design methodology because of the nature of the problem: afferent flow from the input files, new values computed, and efferent flow for the data to the output file (28:265).

The main routine receives all the input information from GSINFO, passes all this to PREP1 which returns the final data (see Figure 3.3 for the overall implementation based on transform analysis). The main routine then passes the final data out to SAVHC which creates the output file.

Keys in the input data determine the geometry of the immobile zone, and the choice of finite differences or finite elements in the mobile zone. These possibilities quite naturally fall out as transactions (28:275). Figure 3.4 shows the transaction analysis, with PREP1 as the transaction center and several choices beneath it for the different possibilities mentioned above.

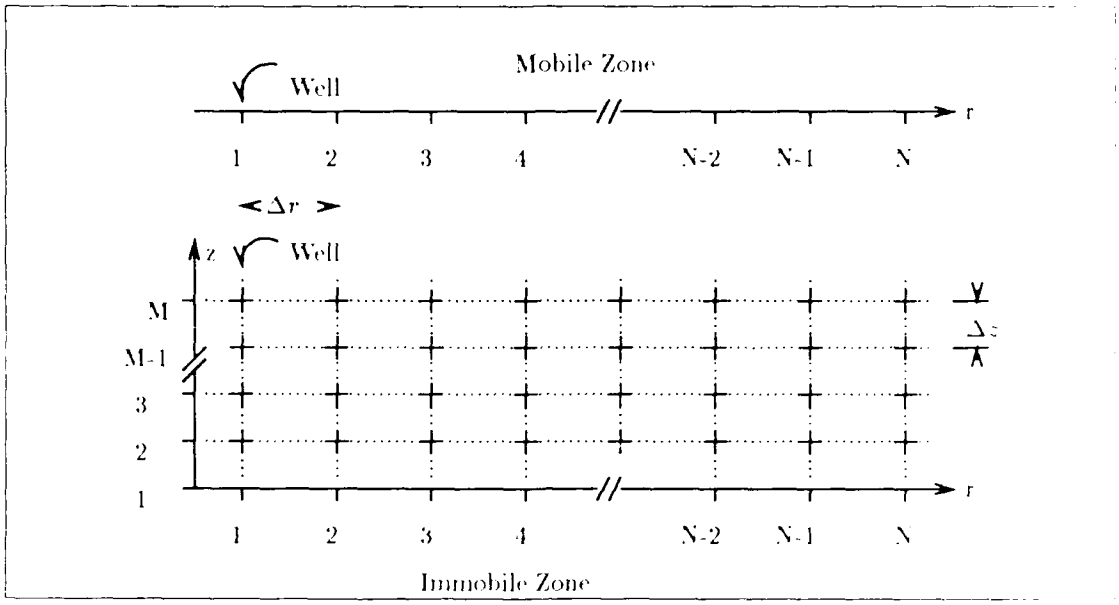

Figure 3.1. Grid Layout for the Mobile and Immobile Zones in the Model

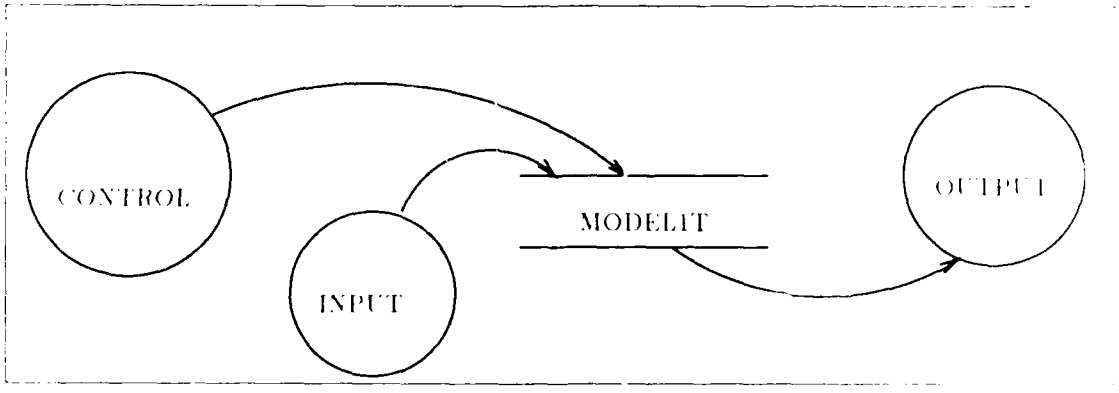

Figure 3.2. Data Flow Diagram for MODELIT

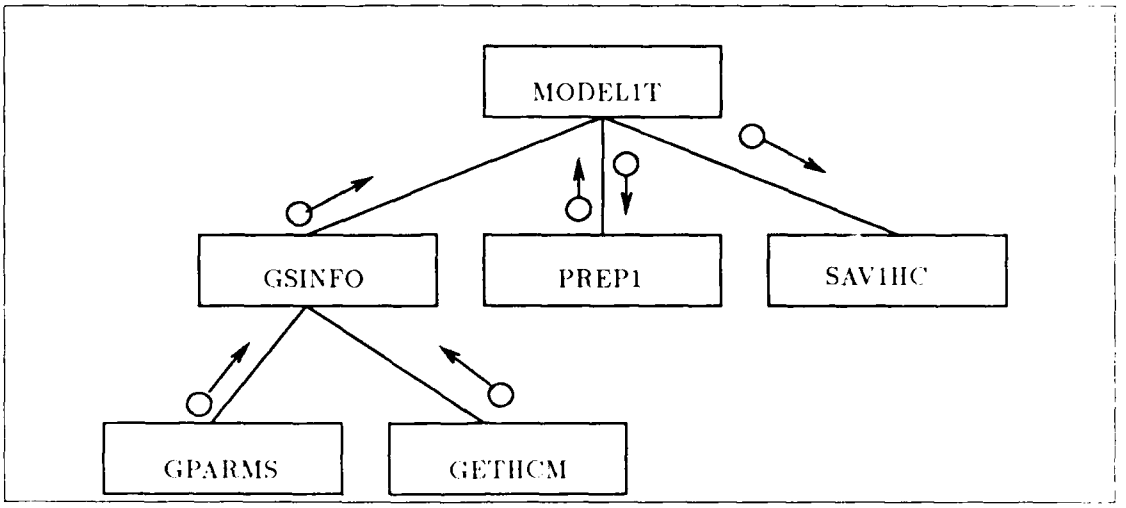

Figure 3.3. MODEL1T Transform Analysis

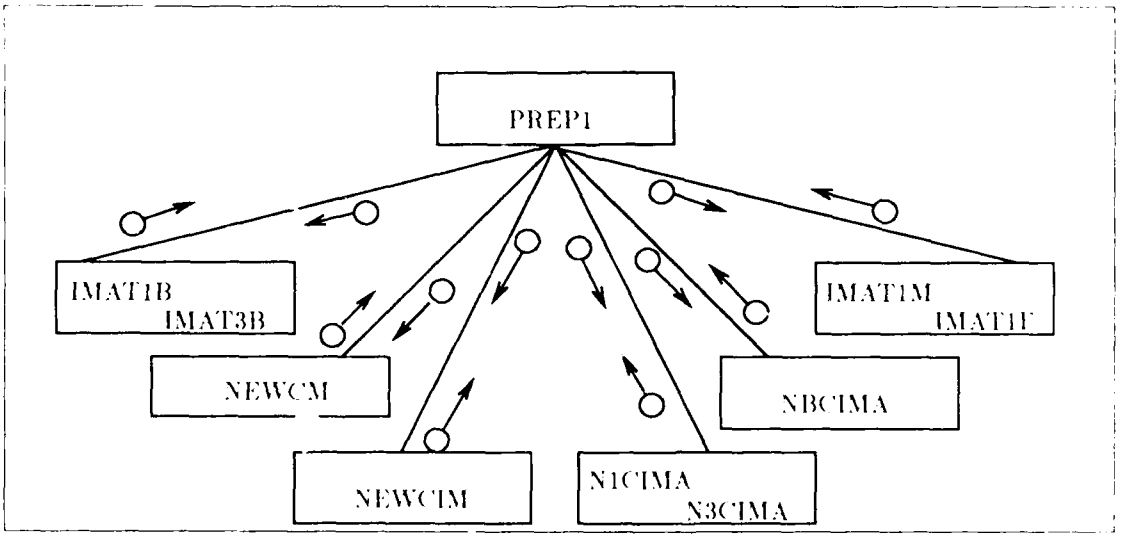

Figure 3.4. MODEL1T Transaction Analysis

3.3 *Numerical Methods*

The following sections describe the procedures employed for mapping the partial differential and integral equations into numerical algorithms.

3.3.1 The Immobile Zone The immobile zone grid (shown in Figure 3.1) is somewhat deceptive: the grid spacing in the radial direction is on the order of meters, while the grid spacing in the z direction is on the order of millimeters. In other words, each column in the immobile zone grid is virtually isolated from every other column. The contaminant diffuses in a column, but not between columns. This should be intuitive because each "column" is actually a representative layered or spherical aggregate of the immobile material.

The immobile zone could consist of spherical aggregates or layers. A column in the immobile zone represents the concentrations in a halfwidth of a layer or the concentration profile along the radius of a typical spherical aggregate, depending on whether we are studying layered or spherical zones, respectively.

3.3.1.1 Diffusion in Layers The derivative on the right hand side of Equation 2.11 is replaced by a numerical approximation based on the Taylor's series expansion about the point w for an arbitrary analytic function $f(w)$:

$$f(w+\Delta w) = f(w) + \frac{\Delta w^1 f'(w)}{1!} + \frac{\Delta w^2 f''(w)}{2!} + \frac{\Delta w^3 f'''(w)}{3!} + \frac{\Delta w^4 f''''(w)}{4!} + \cdots \qquad (3.1)$$

and

$$f(w-\Delta w) = f(w) - \frac{\Delta w^1 f'(w)}{1!} + \frac{\Delta w^2 f''(w)}{2!} - \frac{\Delta w^3 f'''(w)}{3!} + \frac{\Delta w^4 f''''(w)}{4!} - + \cdots \qquad (3.2)$$

These are added and the resulting infinite series truncated to produce the convergent numerical approximation for the second derivative with gridded data

$$f''(w) = \frac{f(w-\Delta w) + 2f(w) + f(w+\Delta w)}{\Delta w^2} + \mathcal{O}(\Delta w^2) \qquad (3.3)$$

With this approximation applied to $\frac{\partial^2 C_{im}(r,z,t)}{\partial z^2}$, Equation 2.11 becomes

$$\frac{\partial C_{im}(r,z,t)}{\partial t} = \frac{D_e}{R_{im}} \frac{C_{im}(r,z-\Delta z,t) + 2C_{im}(r,z,t) + C_{im}(r,z+\Delta z,t)}{\Delta z^2} \tag{3.4}$$

Eliminating the derivative in time by following the method of Crank and Nicolson (38:1075) by integrating from t to $t + \Delta t$:

$$\int_t^{t+\Delta t} \frac{\partial C_{im}(r,z,\tau)}{\partial \tau} d\tau = \int_t^{t+\Delta t} \frac{D_e}{R_{im}} \frac{C_{im}(r,z-\Delta z,\tau) + 2C_{im}(r,z,\tau) + C_{im}(r,z+\Delta z,\tau)}{\Delta z^2} d\tau \tag{3.5}$$

and using the trapezoidal quadrature rule to get C_{im} at the future time:

$$\begin{aligned} C_{im}(r,z,t+\Delta t) &= C_{im}(r,z,t) \\ &+ \Delta t \frac{D_e}{2R_{im}\Delta z^2} \\ &\quad [C_{im}(r,z-\Delta z,t+\Delta t) + 2C_{im}(r,z,t+\Delta t) + C_{im}(r,z+\Delta z,t+\Delta t) \\ &\quad + C_{im}(r,z-\Delta z,t) + 2C_{im}(r,z,t) + C_{im}(r,z+\Delta z,t)] \end{aligned} \tag{3.6}$$

This method also requires boundary conditions for the surfaces of the immobile layers at t and $t + \Delta t$. The values at the boundaries of these layers are the contaminant concentrations in the mobile region.

This implicit method has the following benefits (17:132,152): it is absolutely stable, it does not change amplitude of the physical mode, and has no computational mode! Its drawbacks are the need to do a matrix inversion and it retards the phase slightly. The routines IMAT1B, IMAT3B, IMAT1F, and IMAT1M all create matrices using this method, and invert these matrices once; no further matrix inversions are needed during the execution.

The grid points are numbered with point 1 nearest the mobile zone, and increasing towards the center of the immobile zone. The contaminant concentrations at one side of the immobile zone match those at the other. This is because the concentration in the mobile zone has no vertical component. For this reason, the concentration profile of the contaminant in the immobile layers has a symmetry around the center. Equation 3.6 need only be expanded for the halfwidth,

with a reflection across the center (at $z = 0$). Taking $z = (i-1)\Delta z$ for $i = 1, 2, \cdots, M$ and $C_{im_i}(r,t) = C_{im}(r,[i-1]\Delta z, t)$, the matrix form of Equation 3.6 is:

$$B_1 \underline{C_{im}}(r, t+\Delta t) = B_2 \underline{C_{im}}(r,t) + \underline{V_1}(r,t) \tag{3.7}$$

the matrices and vectors are defined as:

$$B_{1_{i,i}} = 1 + \frac{D_e \Delta t}{R_{im} \Delta r^2} \quad i, = 1, 2, \cdots, M-1 \tag{3.8}$$

$$B_{1_{i,i-1}} = \frac{-D_e \Delta t}{2 R_{im} \Delta r^2} \quad i, = 2, 3, \cdots, M \tag{3.9}$$

$$B_{1_{i,-1,i}} = \frac{-D_e \Delta t}{2 R_{im} \Delta r^2} \quad i, = 2, 3, \cdots, M \tag{3.10}$$

$$B_{2_{i,i}} = 1 - \frac{D_e \Delta t}{R_{im} \Delta r^2} \quad i, = 1, 2, \cdots, M-1 \tag{3.11}$$

$$B_{2_{i,i-1}} = \frac{D_e \Delta t}{2 R_{im} \Delta r^2} \quad i, = 2, 3, \cdots, M \tag{3.12}$$

$$B_{2_{i,-1,i}} = \frac{D_e \Delta t}{2 R_{im} \Delta r^2} \quad i, = 2, 3, \cdots, M \tag{3.13}$$

$$V_{1,}(r,t) = \begin{cases} \dfrac{D_e}{2 R_{im}} \dfrac{\Delta t}{\Delta r^2} \left[C_m(r,t) + C_m(r, t+\Delta t) \right] & i = 1 \\ 0 & otherwise \end{cases} \tag{3.14}$$

The boundary conditions mentioned above are incorporated into the V_1 vector. This scheme requires the knowledge of $C_m(r, t+\Delta t)$ which is not available until after several more procedural steps. An approximation to $C_m(r, t+\Delta t)$ was made using the available data and linear extrapolation:

$$C_m(r, t+\Delta t) = 2 C_m(r,t) - C_m(r, t-\Delta t) \tag{3.15}$$

These equations are implemented in routine IMAT1B in the program.

3.3.1.2 Diffusion in Spheres The form of the Fickian diffusion equation for spheres differs slightly from that for layers. The additional term in Equation 2.13 is:

$$\frac{2}{z} \frac{\partial C_{im}(r,z,t)}{\partial z} \tag{3.16}$$

Using the Taylor's series expansions above (Equations 3.1 and 3.2), and subtracting instead of adding, to obtain the approximation for the first derivative:

$$f'(w) = \frac{f(w+\Delta w) - f(w-\Delta w)}{2\Delta w} + \mathcal{O}(\Delta w^2) \tag{3.17}$$

This is included in Equation 3.4 resulting in:

$$\int_t^{t+\Delta t} \frac{\partial C_{im}(r,z,\tau)}{\partial t} d\tau = \int_t^{t+\Delta t} \frac{D_e}{R_{im}} \left[\frac{C_{im}(r,z-\Delta z,\tau) + 2C_{im}(r,z,\tau) + C_{im}(r,z+\Delta z,\tau)}{\Delta z^2} + \frac{1}{z} \frac{C_{im}(r,z+\Delta z,\tau) - C_{im}(r,z-\Delta z,\tau)}{\Delta z} \right] d\tau \tag{3.18}$$

which is integrated using the trapezoidal quadrature rule to obtain the numerical scheme

$$\begin{aligned} C_{im}(r,z,t+\Delta t) &= C_{im}(r,z,t) + \Delta t \frac{D_e}{2R_{im}\Delta z^2} \\ &\quad [C_{im}(r,z-\Delta z,t+\Delta t) + 2C_{im}(r,z,t+\Delta t) + C_{im}(r,z+\Delta z,t+\Delta t) \\ &+ \frac{1}{z}(C_{im}(r,z+\Delta z,t+\Delta t) - C_{im}(r,z-\Delta z,t+\Delta t)) \\ &+ C_{im}(r,z-\Delta z,t) + 2C_{im}(r,z,t) + C_{im}(r,z+\Delta z,t) \\ &+ \frac{1}{z}(C_{im}(r,z+\Delta z,t) - C_{im}(r,z-\Delta z,t))\Big] \end{aligned} \tag{3.19}$$

In vector form this is identical to Equation 3.7 with slightly different constituents for the matrices.

$$B_{1_{i,i}} = \left(1 + \frac{D_e \Delta t}{R_{im} h^2}\right), \quad i = 2,3,\cdots,M \tag{3.20}$$

$$B_{1_{i,i-1}} = \frac{-D_e \Delta t}{2R_{im}h^2}\left(\frac{i-2}{i-1}\right) \quad i = 2,3,\cdots,M-1 \tag{3.21}$$

$$B_{1_{i,i+1}} = \frac{-D_e \Delta t}{2R_{im}h^2}\left(\frac{i}{i-1}\right) \quad i = 2,3,\cdots,M-1 \tag{3.22}$$

$$B_{2_{i,i}} = \left(1 - \frac{D_e \Delta t}{R_{im} h^2}\right) \quad i = 2,3,\cdots,M-1 \tag{3.23}$$

$$B_{2_{i,i-1}} = \frac{D_e \Delta t}{2R_{im}h^2}\left(\frac{i-2}{i-1}\right) \quad i = 2,3,\cdots,M-1 \tag{3.24}$$

$$B_{2_{i,i+1}} = \frac{D_e \Delta t}{2R_{im}h^2}\left(\frac{i}{i-1}\right) \quad i = 2,3,\cdots,M-1 \tag{3.25}$$

$$V_{1_i}(r,t) = \begin{cases} \dfrac{D_e \Delta t}{2 R_{im} \Delta z^2} \left[C_m(r,t) + C_m(r, t+\Delta t) \right] & \text{i} = 1 \\ 0 & \text{otherwise} \end{cases} \tag{3.26}$$

When $i = 1$ these formulas can not be computed, but the first grid point in the mobile region begins $.1\Delta r$ from the well, yielding a slightly different value for the $B_{1_{2,1}}$, $B_{1_{1,2}}$, $B_{2_{2,1}}$, and $B_{2_{1,2}}$ components. This is implemented in routine IMAT3B in the program.

3.3.2 The Volumetric Averaging To get the time-rate-of-change of the pollutant concentration in the immobile zone we integrate over the halfwidth of the layer or over the radius of the sphere. This change is what makes its way into the mass balance equation (Equation 2.6) to account for the chemicals entering and leaving the mobile zone. The equation governing the volumetric averaging (Equation 2.10) is approximated for each of the two types of immobile zones by the quadrature formula known as Simpson's rule (38:369).

3.3.2.1 Volumetric Averaging in Layers Equation 2.12 gives the volumetric average of the pollutant in a typical layer of the immobile zone. The layered medium provides the simplest form of Equation 2.10 and the conversion of this integral to a numerical quadrature is straightforward. Simpson's rule requires an odd number of points. For example, given a function f which is integrable on the interval $[a, b]$:

$$I = \int_a^b f(w)\, dw \tag{3.27}$$

$$I \doteq \frac{(b-a)}{3} \left[f(a) + 4f\left(\frac{b+a}{2}\right) + f(b) \right] \tag{3.28}$$

$$I \doteq \frac{(b-a)}{6} \left[f(a) + 4f\left(a + \frac{(b-a)}{4}\right) + 2f\left(a + \frac{2(b-a)}{4}\right) + 4f\left(a + \frac{3(b-a)}{4}\right) + f(b) \right] \tag{3.29}$$

But with symmetry about the origin, the number of grid points in a column in the immobile zone can be even or odd. The point at $z = 0$ is the center point in the region, with grid points extending in both directions, necessitating an odd number of points total. The algorithm implemented in NICIMA makes use of this argument to integrate over the halfwidth.

3.3.2.2 Volumetric Averaging in Spheres The argument for spheres is almost the same as that for layers, except that here the number of grid points requested in the immobile region must be odd. The model checks to make sure the requested number of grid points will work with this algorithm in the GSINFO routine.

The integrand of Equation 2.14 contains a z^2 term which complicates matters slightly. The center-most grid point of a sphere doesn't contribute to the total volumetric average, as is shown in this example formula where $\Delta z = \frac{b}{4}$ (i.e., 5 grid points in the immobile zone):

$$I \doteq \frac{\Delta z}{b^3}\left[f(b) + 4f(3\Delta z) + 2f(2\Delta z) + 4f(\Delta z) + f(0)\right] \tag{3.30}$$

where $f(z) = z^2 C_{im}(r, z, t)$ for fixed r and t, and the result is

$$I \doteq \frac{\Delta z}{b^3}\quad \left[b^2 C_{im}(r, b, t) + 4(3\Delta z)^2 C_{im}(r, 3\Delta z, t) + 2(2\Delta z)^2 C_{im}(r, 2\Delta z, t) + \right.$$
$$\left. 4(\Delta z)^2 C_{im}(r, \Delta z, t) + (0\Delta z)^2 C_{im}(r, 0, t)\right] \tag{3.31}$$

3.3.3 The Mobile Zone Mass Balance Equation The mass balanced equation (Equation 2.6) is solved numerically by two methods, the finite element method and finite differences. The finite differences are easier to understand, and were implemented as a check against the finite elements. Comparisons of these two methods with the same input data are made in Chapter 4.

3.3.3.1 Finite Differences in the Mobile Region The procedures for the finite difference method involve replacing the derivates in the equation with approximations to the derivatives based on Taylor's series expansions. The partial derivatives with respect to r of Equation 2.6 are replaced by

$$\frac{\partial^2 C_m(r,t)}{\partial r^2} \doteq \left[\frac{C_m(r-\Delta r, t) + 2C_m(r,t) + C_m(r+\Delta r, t)}{\Delta r^2}\right] \tag{3.32}$$

$$\frac{\partial C_m(r,t)}{\partial r} \doteq \left[\frac{C_m(r+\Delta r, t) - C_m(r-\Delta r, t)}{2\Delta r}\right] \tag{3.33}$$

resulting in

$$\frac{\partial C_m(r,t)}{\partial t} + \frac{\theta_{im} R_{im}}{\theta_m R_m}\frac{\partial C_{ima}(r,t)}{\partial t} \quad =$$

$$\frac{A_l|V(r)|}{R_m}\left[\frac{C_m(r-\Delta r,t)+2C_m(r,t)+C_m(r+\Delta r,t)}{\Delta r^2}\right] - \frac{V(r)}{R_m}\left[\frac{C_m(r+\Delta r,t)-C_m(r-\Delta r,t)}{2\Delta r}\right] \quad (3.34)$$

Integrating this from t to $t+\Delta t$ and rearranging yields:

$$\begin{aligned} C_m(r,t+\Delta t) &= C_m(r,t) \\ &- \frac{\theta_{im}R_{im}}{\Delta t\,\theta_m R_m}\left[C_{ima}(r,t+\Delta t)-C_{ima}(r,t)\right] \\ &+ \frac{\Delta t}{2}\left[\frac{A_l|V(r)|}{R_m}\right. \\ &\quad \left(\frac{C_m(r-\Delta r,t+\Delta t)+2C_m(r,t+\Delta t)+C_m(r+\Delta r,t+\Delta t)}{\Delta r^2}\right) \\ &- \frac{V(r)}{R_m}\left(\frac{C_m(r+\Delta r,t+\Delta t)-C_m(r-\Delta r,t+\Delta t)}{2\Delta r}\right) \\ &+ \frac{A_l|V(r)|}{R_m}\left(\frac{C_m(r-\Delta r,t)+2C_m(r,t)+C_m(r+\Delta r,t)}{\Delta r^2}\right) \\ &- \left.\frac{V(r)}{R_m}\left(\frac{C_m(r+\Delta r,t)-C_m(r-\Delta r,t)}{2\Delta r}\right)\right] \end{aligned} \quad (3.35)$$

Taking $r=(i-1)\Delta r$ for $i=1,2,\cdots,N$ in this equation gives the vector equation:

$$P_1\,\underline{C_m}(t+\Delta t) = P_2\,\underline{C_m}(t) - \frac{\beta}{\Delta t}\left[\underline{C_{ima}}(t+\Delta t)-\underline{C_{ima}}(t)\right] \quad (3.36)$$

where $\beta=\dfrac{\theta_{im}R_{im}}{\theta_m R_m}$ and $C_{m_i}(t)=C_m([i-1]\Delta r,t)$ for $i=1,2,\cdots,N$.

The values for $C_{ima}(r,t)$ are available at $t+\Delta t$ because they depend upon $C_{im}(r,z,t)$ only, and the algorithm makes the linear extrapolation to approximate $C_m(r,t+\Delta t)$. The tri-diagonal matrices P_1 and P_2 are initialized in routine IMAT1F, and individual components of these matrices are defined here:

$$P_{1_{i,i-1}} = -\frac{(\zeta+\xi)}{(i-1)} \quad i=2,3,\cdots,N-1 \quad (3.37)$$

$$P_{1_{i,i}} = -\frac{(2\zeta)}{(i-1)}+\frac{1}{\Delta t} \quad i=2,3,\cdots,N-1 \quad (3.38)$$

$$P_{1_{i,i+1}} = \frac{(-\zeta+\xi)}{(i-1)} \quad i=2,3,\cdots,N-1 \quad (3.39)$$

$$P_{2_{i,i-1}} = \frac{(\zeta+\xi)}{(i-1)} \quad i=2,3,\cdots,N-1 \quad (3.40)$$

$$P_{2_{i,i}} = \frac{(2\zeta)}{(i-1)} + \frac{1}{\Delta t} \quad i = 2, 3, \cdots, N-1 \tag{3.41}$$

$$P_{2_{i,i+1}} = -\frac{(-\zeta + \xi)}{(i-1)} \quad i = 2, 3, \cdots, N-1 \tag{3.42}$$

with $\zeta = \frac{A_l \, |Q_w|}{4 \, R_m \, \pi \, H \, \theta_m \, (\Delta r)^3}$ and $\xi = \frac{Q_w}{2 \, R_m \, \pi \, H \, \theta_m}$. The values in the first row of each of these matrices differs slightly because the grid begins $.1\Delta r$ out from the well.

3.3.3.2 Finite Elements in the Mobile Region The finite element method employed here uses the chapeau function (also known as the 'roof' or 'hat' function (17:183) (31:27), see Figure 3.5). The first two functions in the series deviate slightly because of the restriction at the well, where the formula for induced water velocity (Equation 2.2) has a singularity. The basis

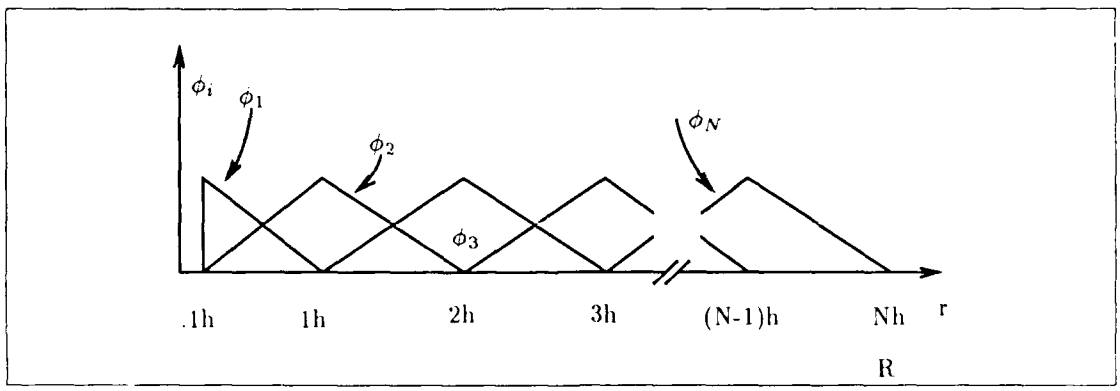

Figure 3.5. FEM Basis Functions for the Mobile Region

functions are

$$\phi_1(r) = \begin{cases} \frac{-r}{0.9h} + \frac{1}{0.9} & (0.1)h \le r \le h \\ 0 & otherwise \end{cases} \tag{3.43}$$

$$\phi_2(r) = \begin{cases} \frac{r}{0.9h} - \frac{1}{9.} & (0.1)h \le r \le h \\ \frac{-r}{h} + 2 & h \le r \le 2h \\ 0 & otherwise \end{cases} \tag{3.44}$$

And for $i \in \{3, 4, \cdots, N\}$:

$$\phi_i(r) = \begin{cases} \dfrac{r}{h} - (i-2) & (i-2)h \le r \le (i-1)h \\ \dfrac{-r}{h} + i & (i-1)h \le r \le (i)h \\ 0 & otherwise \end{cases} \tag{3.45}$$

$$\phi_{i+1}(r) = \begin{cases} \dfrac{r}{h} - (i-1) & (i-1)h \le r \le (i)h \\ \dfrac{-r}{h} + (i+1) & (i)h \le r \le (i+1)h \\ 0 & otherwise \end{cases} \tag{3.46}$$

$$\phi_{i-1}(r) = \begin{cases} \dfrac{r}{h} - (i-3) & (i-3)h \le r \le (i-2)h \\ \dfrac{-r}{h} + (i-1) & (i-2)h \le r \le (i-1)h \\ 0 & otherwise \end{cases} \tag{3.47}$$

with derivatives

$$\phi_1'(r) = \begin{cases} \dfrac{-1}{0.9h} & (0.1)h < r < h \\ 0 & otherwise \end{cases} \tag{3.48}$$

$$\phi_2'(r) = \begin{cases} \dfrac{1}{0.9h} & (0.1)h < r < h \\ \dfrac{-1}{h} & h < r < 2h \\ 0 & otherwise \end{cases} \tag{3.49}$$

$$\phi_i'(r) = \begin{cases} \dfrac{1}{h} & (i-2)h < r < (i-1)h \\ \dfrac{-1}{h} & (i-1)h < r < (i)h \\ 0 & otherwise \end{cases} \tag{3.50}$$

$$\phi_{i+1}'(r) = \begin{cases} \dfrac{1}{h} & (i-1)h < r < (i)h \\ \dfrac{-1}{h} & (i)h < r < (i+1)h \\ 0 & otherwise \end{cases} \tag{3.51}$$

$$\phi_{i-1}'(r) = \begin{cases} \dfrac{1}{h} & (i-3)h < r < (i-2)h \\ \dfrac{-1}{h} & (i-2)h < r < (i-1)h \\ 0 & otherwise \end{cases} \tag{3.52}$$

Taking Equation 2.6 and multiplying by $\phi_j(r)$ for each $j = 1, 2, \cdots, N$ and integrating with respect to r over the domain [0,R] yields:

$$\begin{aligned}\int_0^R \frac{\partial C_m(r,t)}{\partial t}\phi_j(r)dr &= \frac{A_l}{R_m}\int_0^R |V(r)|\frac{\partial^2 C_m(r,t)}{\partial r^2}\phi_j(r)dr \\ &- \frac{1}{R_m}\int_0^R V(r)\frac{\partial C_m(r,t)}{\partial r}\phi_j(r)dr \\ &- \beta\int_0^R \frac{\partial C_{ima}(r,t)}{\partial t}\phi_j(r)dr \quad \text{for} \quad i = 1, 2, \cdots, N \end{aligned} \tag{3.53}$$

Integration by parts of the second derivative term produces:

$$\begin{aligned}\int_0^R |V(r)|\frac{\partial^2 C_m(r,t)}{\partial r^2}\phi_j(r)dr &= |V(r)|\frac{\partial C_m(r,t)}{\partial r}\phi_j(r)\Big|_0^R \\ &- \int_0^R \frac{\partial C_m(r,t)}{\partial r}\phi_j'(r)|V(r)|dr \\ &- \int_0^R \frac{\partial C_m(r,t)}{\partial r}\phi_j(r)|V'(r)|dr \end{aligned} \tag{3.54}$$

Applying the definition of the $\phi_j(r)$ eliminates the evaluation term. Substituting this result back into Equation 3.53 yields:

$$\begin{aligned}\int_0^R \frac{\partial C_m(r,t)}{\partial t}\phi_j(r)dr &= -\frac{A_l}{R_m}\int_0^R \frac{\partial C_m(r,t)}{\partial r}\phi_j'(r)|V(r)|dr \\ &- \frac{A_l}{R_m}\int_0^R \frac{\partial C_m(r,t)}{\partial r}\phi_j(r)|V'(r)|dr \\ &- \frac{1}{R_m}\int_0^R V(r)\frac{\partial C_m(r,t)}{\partial r}\phi_j(r)dr \\ &- \beta\int_0^R \frac{\partial C_{ima}(r,t)}{\partial t}\phi_j(r)dr \quad \text{for } j = 1, 2, \cdots, N \end{aligned} \tag{3.55}$$

The variables $C_m(r,t)$ in this equation are replaced by the chapeau functions shown above:

$$C_m(r,t) \doteq \sum_{i=1}^{N} \alpha_i(t)\phi_i(r) \tag{3.56}$$

giving:

$$\begin{aligned}\int_0^R \sum_{i=1}^{N} \alpha_i'(t)\phi_i(r)\phi_j(r)dr &= -\frac{A_l}{R_m}\int_0^R \sum_{i=1}^{N} \alpha_i(t)\phi_i'(r)\phi_j'(r)|V(r)|dr \\ &- \frac{A_l}{R_m}\int_0^R \sum_{i=1}^{N} \alpha_i(t)\phi_i'(r)\phi_j(r)|V'(r)|dr \end{aligned}$$

$$- \frac{1}{R_m}\int_0^R \sum_{i=1}^{N} \alpha_i(t)\phi_i'(r)\phi_j(r)V(r)dr$$

$$- \beta\int_0^R \frac{\partial C_{ima}(r,t)}{\partial t}\phi_j(r)dr \qquad (3.57)$$

for $j = 1, 2, \cdots, N$. This produces:

$$\mathcal{A}_1\,\underline{\alpha}' + \beta\int_0^R \frac{\partial C_{ima}(r,t)}{\partial t}\underline{\phi}(r)dr = -\frac{A_l}{R_m}\mathcal{A}_2\,\underline{\alpha} - \frac{A_l}{R_m}\mathcal{A}_3\,\underline{\alpha} - \frac{1}{R_m}\mathcal{A}_4\underline{\alpha} \qquad (3.58)$$

where $\underline{\alpha}(t) = [\alpha_1(t), \alpha_2(t), \ldots, \alpha_N(t)]^T$ and $\underline{\alpha}'(t) = [\alpha_1'(t), \alpha_2'(t), \ldots, \alpha_N'(t)]^T$, and the basis function vector $\underline{\phi}(r) = [\phi_1(r), \phi_2(r), \cdots, \phi_N(r)]^T$, with the matrix components for the four matrices $\mathcal{A}_1, \mathcal{A}_2, \mathcal{A}_3$, and $\mathcal{A}_4$ defined:

$$\mathcal{A}_{1_{i,j}} = \int_0^R \phi_i(r)\phi_j(r)dr \qquad i = 1, 2, \cdots, N \quad j = 1, 2, \cdots, N \qquad (3.59)$$

$$\mathcal{A}_{2_{i,j}} = \int_0^R \phi_i'(r)\phi_j'(r)|V(r)|dr \quad i = 1, 2, \cdots, N \quad j = 1, 2, \cdots, N \qquad (3.60)$$

$$\mathcal{A}_{3_{i,j}} = \int_0^R \phi_i'(r)\phi_j(r)|V'(r)|dr \quad i = 1, 2, \cdots, N \quad j = 1, 2, \cdots, N \qquad (3.61)$$

$$\mathcal{A}_{4_{i,j}} = \int_0^R \phi_i'(r)\phi_j(r)V(r)dr \quad i = 1, 2, \cdots, N \quad j = 1, 2, \cdots, N \qquad (3.62)$$

The method of Crank-Nicolson (trapezoidal quadrature for the time derivative) is used to remove the integration in time to obtain:

$$\left[\frac{\mathcal{A}_1}{\Delta t} + \frac{A_l}{2R_m}(\mathcal{A}_2 + \mathcal{A}_3) + \frac{\mathcal{A}_4}{2R_m}\right]\underline{\alpha}(t+\Delta t) = \left[\frac{\mathcal{A}_1}{\Delta t} - \frac{A_l}{2R_m}(\mathcal{A}_2 + \mathcal{A}_3) - \frac{\mathcal{A}_4}{2R_m}\right]\underline{\alpha}(t)$$
$$- \beta\int_0^R \frac{\partial C_{ima}(r,t)}{\partial t}\underline{\phi}(r)dr \qquad (3.63)$$

which is further simplified by defining

$$Q_1 = \left[\frac{\mathcal{A}_1}{\Delta t} + \frac{A_l}{2R_m}(\mathcal{A}_2 + \mathcal{A}_3) + \frac{\mathcal{A}_4}{2R_m}\right] \qquad (3.64)$$

and

$$Q_2 = \left[\frac{\mathcal{A}_1}{\Delta t} - \frac{A_l}{2R_m}(\mathcal{A}_2 + \mathcal{A}_3) - \frac{\mathcal{A}_4}{2R_m}\right] \qquad (3.65)$$

yielding:

$$Q_1\underline{\alpha}(t+\Delta t) = Q_2\underline{\alpha}(t) - 3\int_0^R \frac{\partial C_{ima}(r,t)}{\partial t}\underline{\phi}(r)dr \qquad (3.66)$$

These matrices are initialized in routine IMAT1M in the program MODEL1T. (see Part 2 of this Thesis).

IV. Results

4.1 Introduction

This chapter presents an evaluation of the computer model developed in Chapter 3. Since there exists a paucity of suitable field data for comparison, comparison will be made with the transform solution provided by Dr. Goltz. An internal comparison will also be presented to demonstrate the relative effect of the advection, dispersion, and diffusion mechanisms.

The results of several executions are presented here. The model execution produces enormous quantities of data that almost require graphical depictions to make them understandable. The following sections include many such pictures showing the progress and fate of the contaminant. In many instances, the output from one execution is fed back into the next execution to demonstrate the feasibility of simulating pulse pumping.

4.2 Comparison With the Analytic Solution

The computer model solves the same equation set used by Goltz, but surpasses the abilities of his solution by allowing arbitrary initial conditions, and pulse pumping. The cost of this added flexibility is the accuracy of the solution as time progresses. With identical initial data both models should produce similar results. The analytic solution solves the problem for all times simultaneously, and the numerical solution steps forward in time, and is, therefore, subject to compounding errors.

4.2.1 Layered Immobile Material. The results of one comparison are shown in Table 4.1, where the column labeled "FEM" is the finite element solution, the column labeled "FDM" is finite differences, and the "Anal" is the analytic solution provided by Goltz (13). These values are the concentration of the pollutant at the well.

The initial contaminant concentration distribution was a constant 1.0 out 28 meters from the well center and then downward to a value of 0.0 for both mobile and immobile zones. The immobile zone type was 'layered', the other input data is shown in Table 4.2.

The "FEM" solution is reasonably close to the analytic solution, and in fact, only deviates by 0.74% at 100 days! The "FEM" solution more closely resembled the analytic solution than the

Table 4.1. Layered Immobile Material Comparison Test

Day	Anal	FEM	FDM	Day	Anal	FEM	FDM
0	1.000	1.000	1.000	32	.5838	.5889	.6647
5	1.000	1.000	1.000	35	.4580	.4525	.5511
10	1.000	.9999	.9998	40	.2978	.2726	.3692
15	.9980	1.002	.9948	45	.1998	.1648	.2261
16	.9991	1.002	.9918	50	.1463	.1115	.1343
17	1.000	1.002	.9876	55	.1188	.0896	.0891
18	1.001	1.001	.9821	60	.1045	.0814	.0736
19	.9990	.9976	.9748	65	.0963	.0783	.0722
20	.9937	.9910	.9656	70	.0906	.0766	.0749
21	.9837	.9806	.9541	75	.0859	.0752	.0770
22	.9682	9657	.9404	80	.0816	.0738	.0773
24	.9197	.9213	.9050	85	.0776	.0723	.0762
26	.8504	.8573	.8591	90	.0739	.0708	0745
28	.7663	.7771	.8030	95	.0704	.0693	.0726
30	.6750	.6838	.7364	100	.0673	.0678	.0709

Table 4.2. Input Parameters for the Layered Immobile Material Comparison Test

Q_w	θ	θ_m/θ	D_e	H	ρ	f	b	A_l	K_d
1.16E-2	.42	.5	1.15E-10	10.	1.81E-3	.4	.05	.5	1.48E3

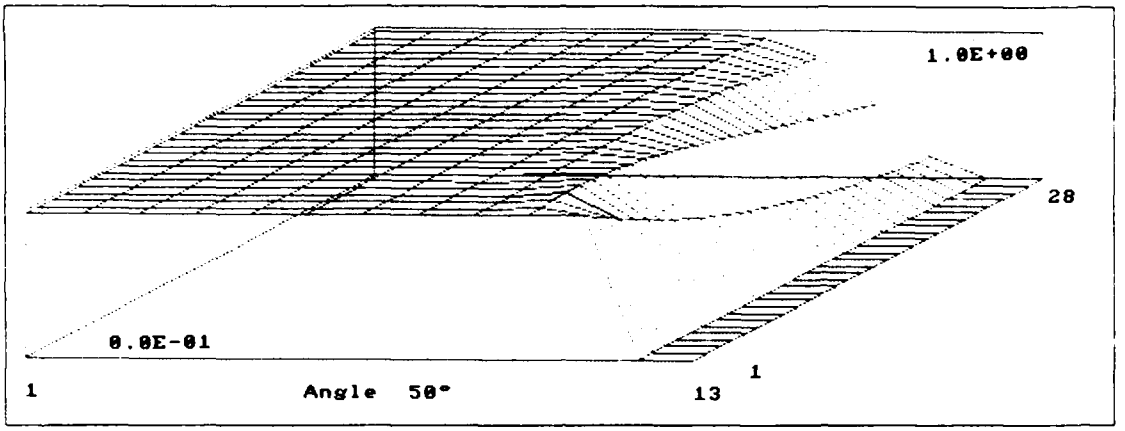

Figure 4.1. Mobile Zone Concentration Progression, Days 0-10, Layered Immobile Material

"FDM" solution. Part of the deviations between these solutions is caused by the initial profile of the concentration. Whereas the analytic solution drops the concentration from 1.0 to 0.0 instantly at $r = R$, the numerical solution drops it linearly between two grid points. This makes it difficult to match the initial conditions, especially when the grid spacing is over 2 meters, as in the first test.

Figures 4.1 through 4.6 show the level of the contaminant in the mobile region as time progresses. Each of these figures represents 10 days time, with the beginning profile in the foreground and ending in the background. The magnitude of the contaminant is shown by the axis of the ordinate and the radial distance out from the well is shown along the axis of the abscissa. The greatest and least levels of the contaminant shown on the graph are printed on the right rear of the projection. The angle of the projection is the angle the perspective appears to make relative to the abscissa. The numbers along the abscissa are the number of grid points in the radial dimension, with 1 being the point at the well boundary. The numbers along the right side of the graph, following the perspective, are the number of iterations displayed (not the number of iterations for the calculations).

As these figures demonstrate, the contaminant is drawn toward the well and extracted, until the level drops below about 10%. From this point onward, the level drops much more slowly, until it appears to level off at around 0.070. Actually, the level is dropping, but the contaminant

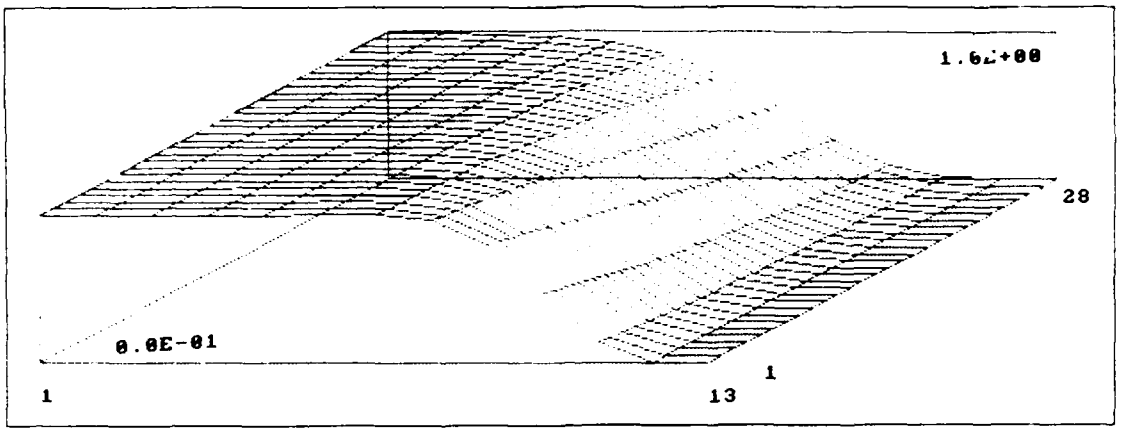

Figure 4.2. Mobile Zone Concentration Progression, Days 10–20, Layered Immobile Material

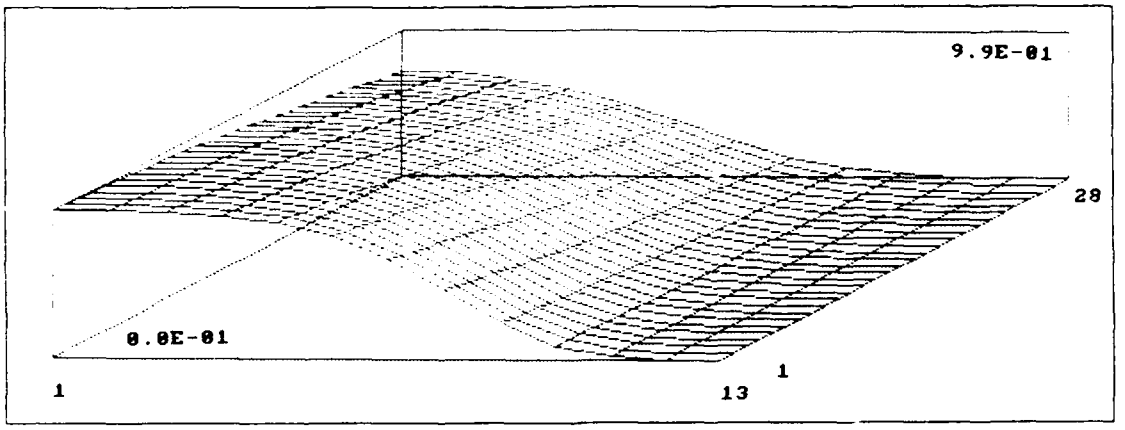

Figure 4.3. Mobile Zone Concentration Progression, Days 20–30, Layered Immobile Material

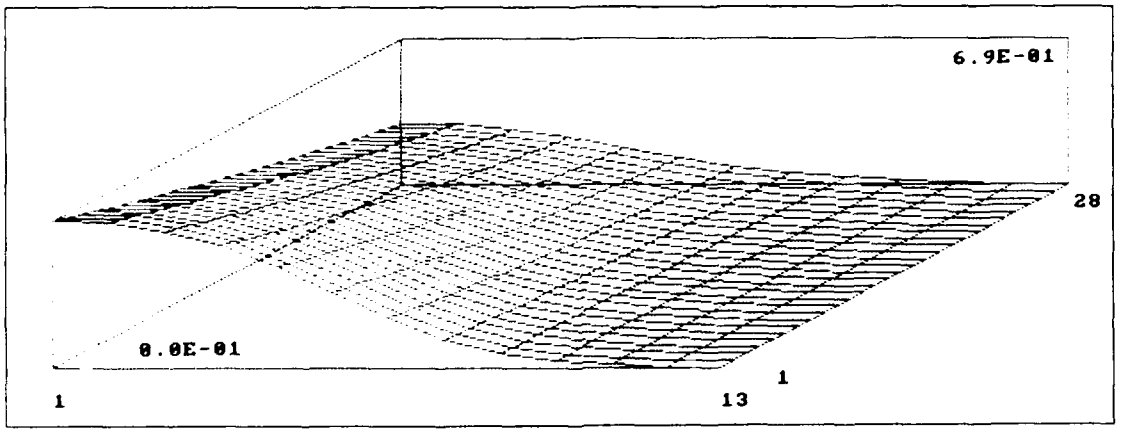

Figure 4.4. Mobile Zone Concentration Progression, Days 30–40, Layered Immobile Material

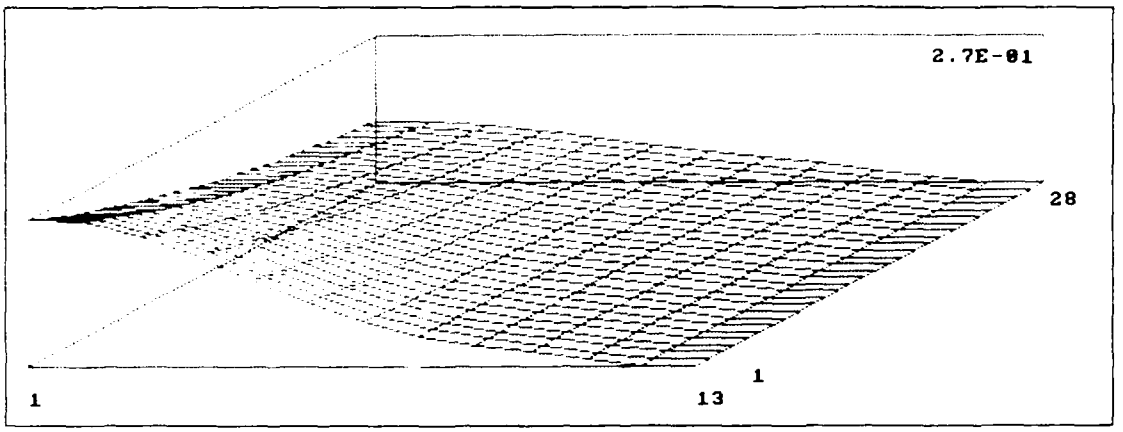

Figure 4.5. Mobile Zone Concentration Progression, Days 40–50, Layered Immobile Material

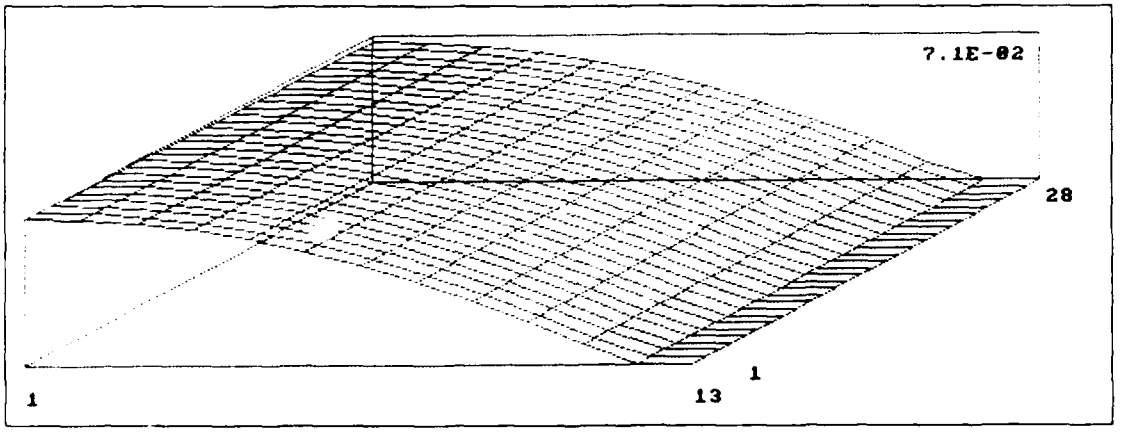

Figure 4.6. Mobile Zone Concentration Progression, Days 90–100, Layered Immobile Material

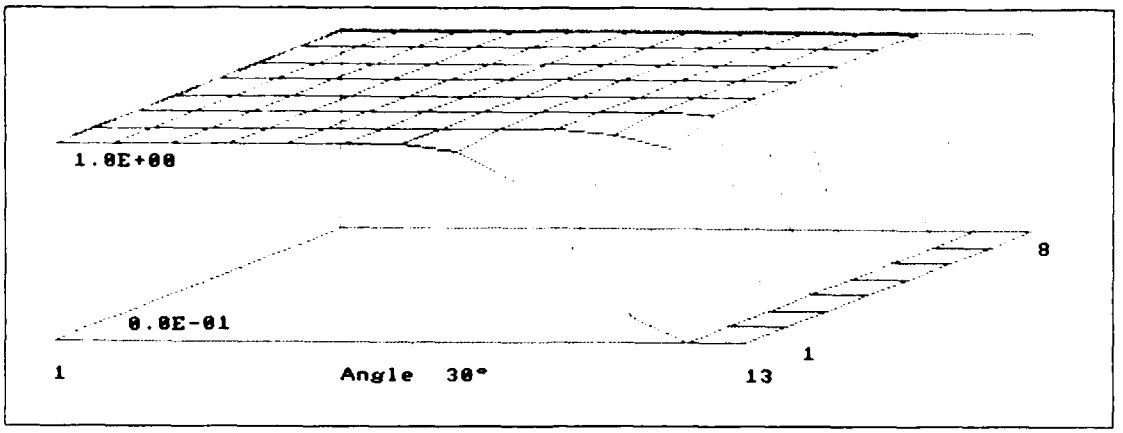

Figure 4.7. Immobile Zone Concentration Profile, Day 10, Layered Immobile Material

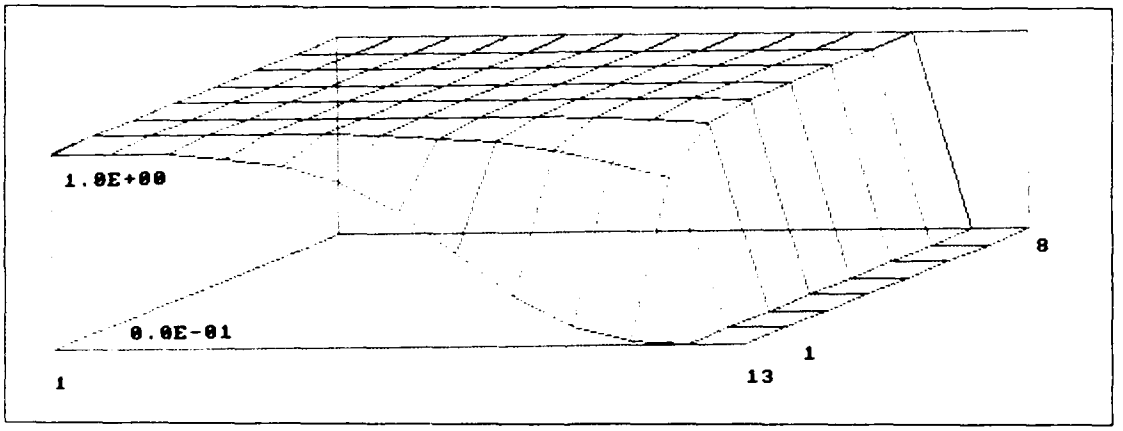

Figure 4.8. Immobile Zone Concentration Profile, Day 20, Layered Immobile Material

that desorbs from the immobile regions feeds the mobile zone. This can be seen more readily by examining Figures 4.7 through 4.12 which display the concentration profiles in the immobile zone at the end of each period indicated.

The level of pollutant in the mobile zone is displayed in the foreground, with the profile for the immobile zone behind it. As the level of the pollutant in the mobile region decreases, the gradient between these two regions increases, as does the flux of chemicals from the immobile zone. At the end of this 100 day test (see Figure 4.12), the levels in the immobile regions are still quite high, and indicate that only a small portion of the total contaminant was removed.

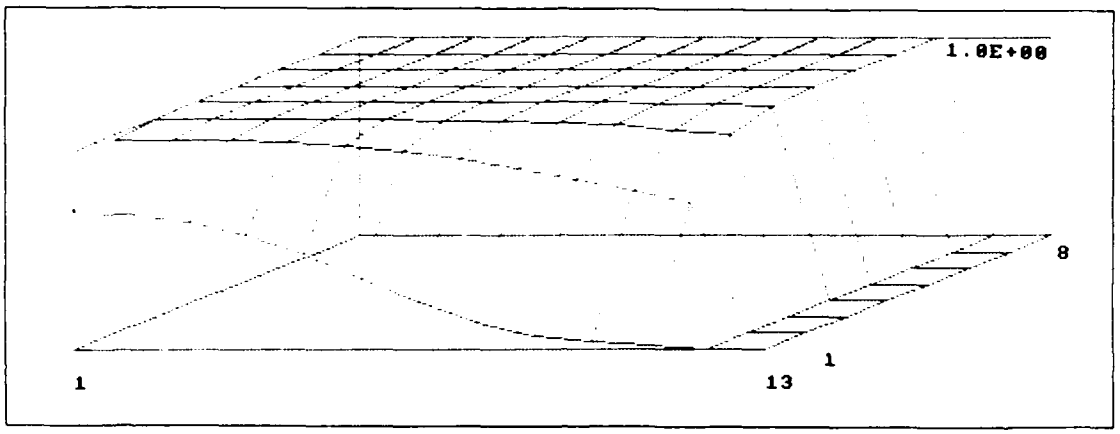

Figure 4.9. Immobile Zone Concentration Profile, Day 30, Layered Immobile Material

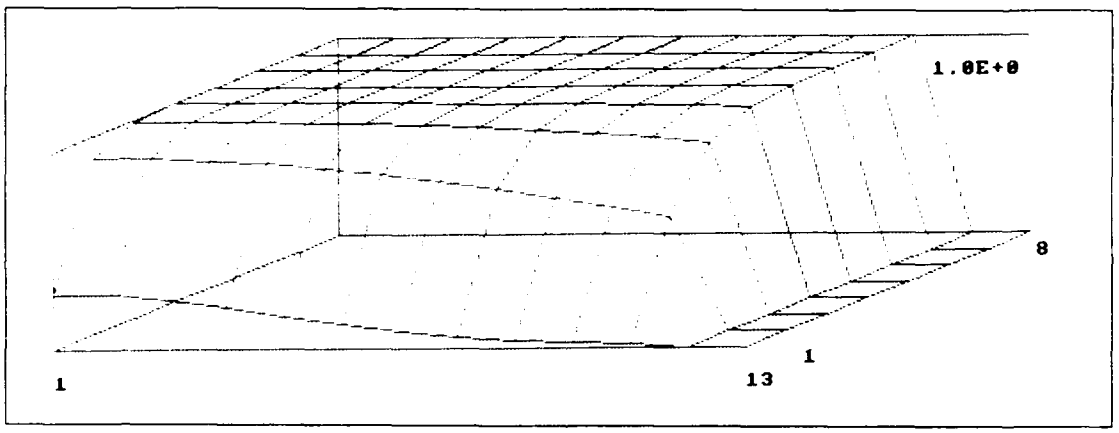

Figure 4.10. Immobile Zone Concentration Profile, Day 40, Layered Immobile Material

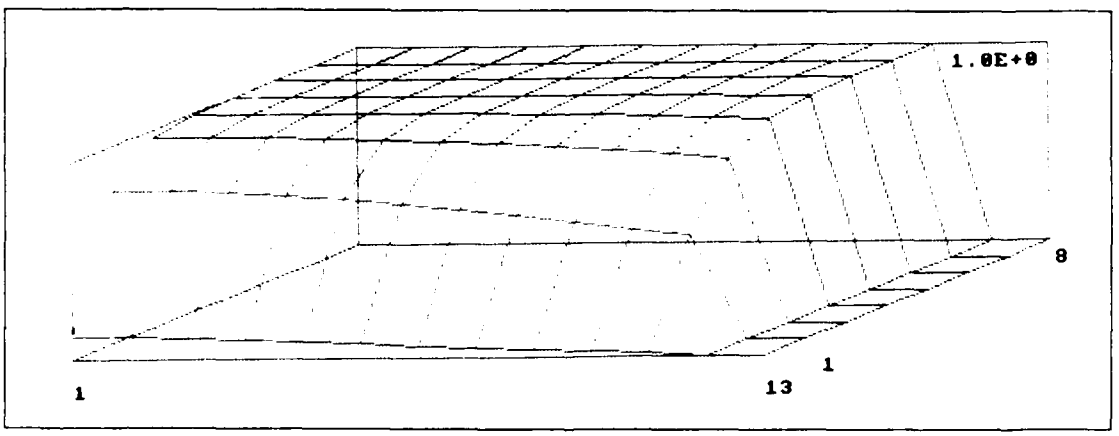

Figure 4.11. Immobile Zone Concentration Profile, Day 50, Layered Immobile Material

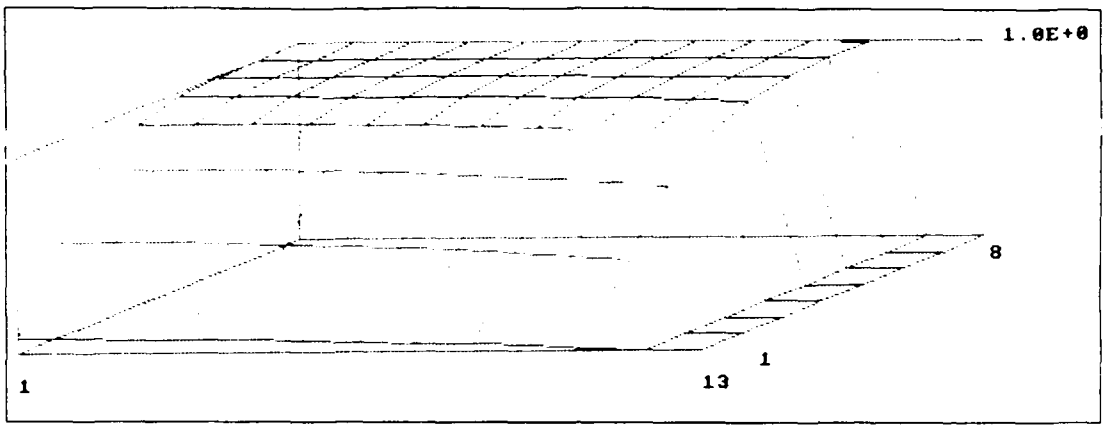

Figure 4.12. Immobile Zone Concentration Profile, Day 100, Layered Immobile Material

Table 4.3. Spherical Immobile Material Comparison Test

Day	Anal	FEM	FDM	Day	Anal	FEM	FDM
0	1.000	1.000	1.000	30	.0381	.0518	.0546
2	1.000	1.000	.9999	40	.0250	.0359	.0377
4	1.000	1.000	.9813	50	.0170	.0258	.0271
6	.8174	.8187	.8343	60	.0116	.0188	.0197
8	.4468	.4493	.5405	70	.0081	.0138	.0145
10	.2257	.2308	.2846	80	.0057	.0101	.0107
15	.0969	.1129	.1159	90	.0038	.0074	.0078
20	.0674	.0821	.0868	100	.0026	.0054	.0058

4.2.2 Spherical Immobile Material This test demonstrates the model's ability to simulate spherical immobile regions. The input parameters used here are given in Table 4.4, and the results of model executions are presented in Table 4.3.

The model presented here agrees favorably with the analytic solution for several days, then begins to show a markedly higher concentration. By the end of the test period, the model predicts about twice as much contaminant at the well as the analytic solution. This is due to the way the model represents spherical immobile material. The radius of a typical sphere, and the number of

Table 4.4. Input Parameters for the Spherical Immobile Material Comparison Test

Q_w	θ	θ_m/θ	D_e	H	ρ	f	b	A_l	K_d
1.16E-2	.42	2/3	1.15E-10	10.	1.81E-3	.4	.05	.5	.0

divisions in the immobile region is input. The sphere radius is divided into even intervals, with the boundary (the mobile region concentration) at the same interval from the boundary of the sphere. This effectively includes the extra interval in the immobile element, and since the extra 'shell' adds a substantial volume to the sphere, the amount of contaminant released by desorption is much greater than expected. For the simple case of four grid points in a sphere, the volume increase is 95%! As the number of grid points increases, this effect is diminished, though as the number of grid points increases in the immobile region, the execution time increases as well.

The concentration in the immobile zone decreases more rapidly when the zone is spherical than when it consists of layers. This is because for the same volume, the spherical aggregates have a much larger surface area in contact with the mobile zone than the layered immobile material. The spherical aggregates have six times as much surface area in contact with the boundary than layered immobile material of the same volume and halfwidth. For instance, with one cubic meter and a halfwidth of 0.05 meters, the surface area for layered immobile material is 10 square meters, and for spherical immobile material is 60 square meters. This also means that the contaminant concentration in the spheres decreases more rapidly than is observed for layered immobile material when all else is identical.

4.3 Advection, Dispersion, and Slow Desorption Tests

The comparison undertaken here is one where the input parameters are adjusted so that the program models advection only, then advection and dispersion, and finally advection, dispersion, and slow desorption. The temporal progressions for these three model executions are shown in Figures 4.13, 4.14, and 4.15, with the concentrations extracted from the well shown in Table 4.6. These three time progressions are displayed with time *decreasing* with the perspective (the opposite of other similar figures in this chapter.) The input parameters are shown in Table 4.5. Advection only is achieved by making the diffusion in the immobile region so small it becomes negligible, and dispersion is eliminated by setting the dispersivity to zero. The model simulated layered immobile material for this test and used finite elements in the mobile zone.

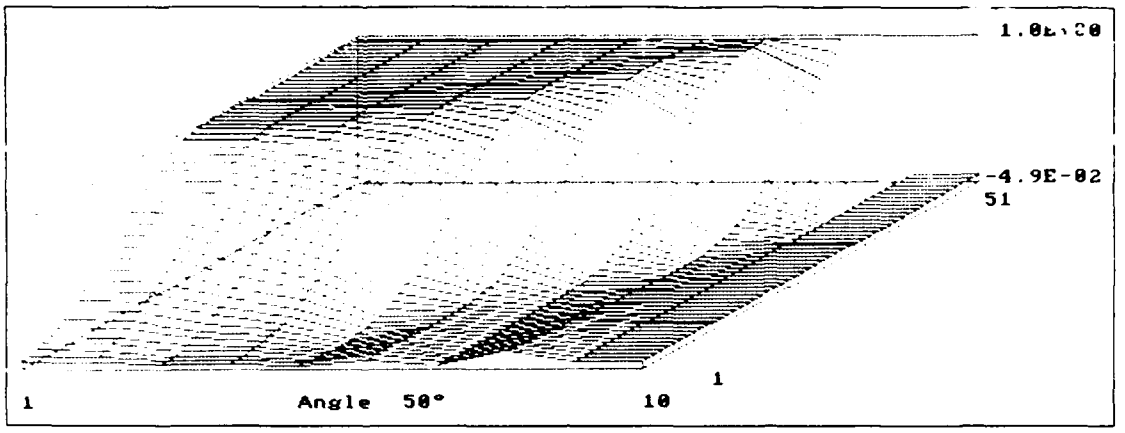

Figure 4.13. Mobile Zone Concentration Profile, Days 0–30, Advection Only (reversed perspective)

With advection only, there should not be a spreading of the contaminant. The sharp drop in contaminant should be advected intact toward the well. However, because of the representation in the model, the top of this gradient is one grid point closer to the well than the bottom of the gradient. This, coupled with the slightly increased water velocity makes the top of this gradient move faster than the bottom.

The model equations do not provide smoothing of the data or require the concentration to be positive in sign. The dispersion induces a smoothing of the data, and prevents spurious negative values from occurring. Unfortunately, when the model simulates advection only, the shock condition from the input profile causes an overshooting that yields negative concentrations. When the input data is devoid of these shock conditions, negative concentrations don't appear.

With advection only, all the contaminant would be removed from the aquifer. When the dispersion coefficient is not zero, the contaminant is spread out and it takes longer to remove the contaminant from the aquifer. By comparing the final profiles in Figures 4.14 and 4.15 and the concentrations extracted from the well (Table 4.6) it is evident that the slow desorption process is especially important in the latter part of the remediation effort.

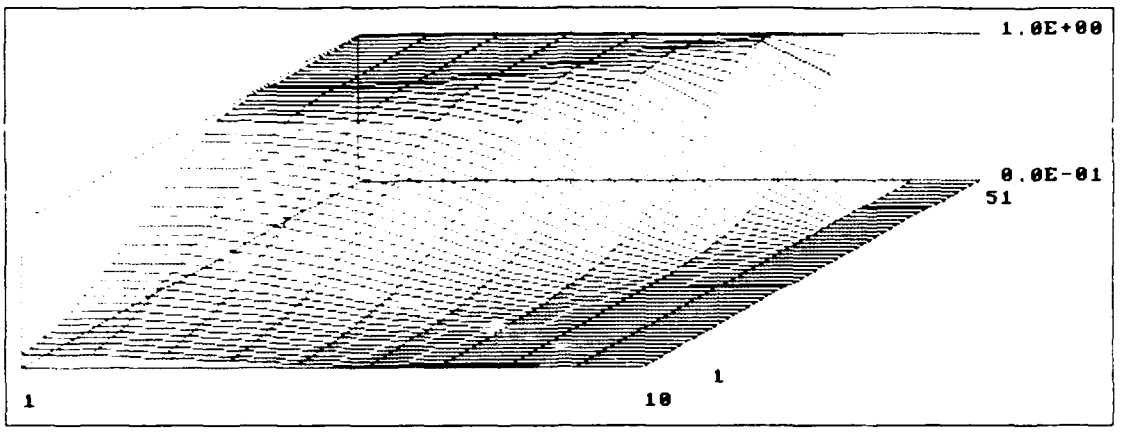

Figure 4.14. Mobile Zone Concentration Profile, Days 0–30, Advection and Dispersion (reversed perspective)

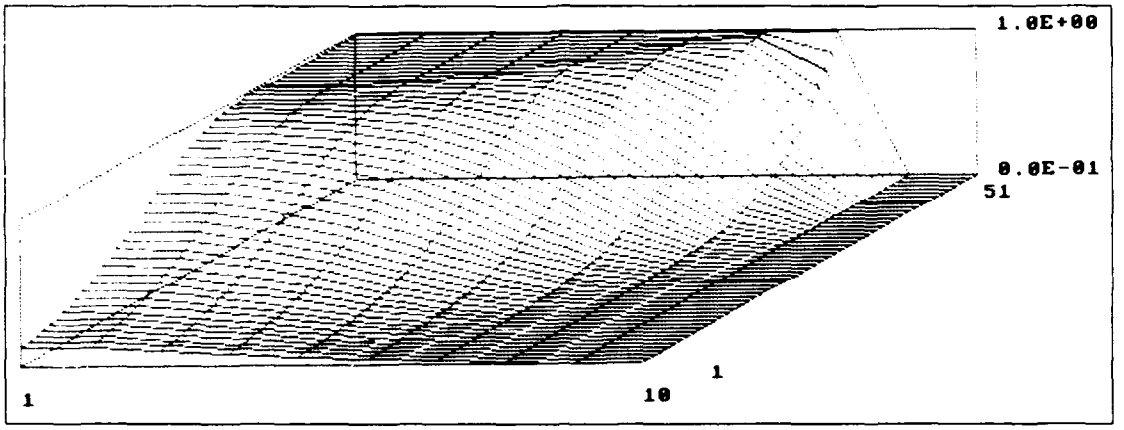

Figure 4.15. Mobile Zone Concentration Profile, Days 0–30, Advection, Dispersion, and Slow Desorption (reversed perspective)

Table 4.5. Input Parameters for the Advection, Dispersion, and Slow Desorption Comparison Test

Test	Q_w	θ	θ_m/θ	D_e	H	ρ	f	b	A_l	K_d
Adv	1.16E-2	.42	.5	1.15E-20	10.	1.81E-3	.4	.05	.0	1.48E3
Adv+Disp	1.16E-2	.42	.5	1.15E-20	10.	1.81E-3	.4	.05	.0	1.48E3
All	1.16E-2	.42	.5	1.15E-10	10.	1.81E-3	.4	.05	.5	1.48E3

Table 4.6. Advection, Dispersion, and Slow Desorption Comparison Test

Day	Adv	Adv+Dis	All	Day	Adv	Adv+Dis	All
0	1.000	1.000	1.000	16	.9454	.7179	.7845
2	.9999	1.000	1.000	18	.9268	.6414	.6520
4	1.000	.9998	.9998	20	.6582	.5002	.5164
6	.9995	.9999	.9999	22	.4670	.3708	.3929
8	.9988	1.004	1.004	24	.2854	.2623	.2900
10	1.004	1.001	1.001	26	.1357	.1755	.2084
12	1.013	.9693	.9698	28	.0401	.1141	.1511
14	1.004	.8955	.8980	30	-.001	.0714	.1117

4.4 Pulse Pumping

The first test above had a duration of 100 days. In this section looks at the continuation of that test out to 400 days with different pumping rates. In this first test (Pulse Pumping Test 1) the pumping rate was one cubic meter per day for the remaining 300 days (see Figure 4.16). In the next test (Pulse Pumping Test 2) the pumping rate was one cubic meter per day for days 100 to 200, then at 1000 cubic meters per day (the value used in the first test in this chapter) from day 200 to 300, and then back to one cubic meter per day for the last 100 days (see Figure 4.17). In the final example (Pulse Pumping Test 3) the pumping rate was 50 cubic meters p day for the entire period from day 100 to day 400 (see Figure 4.18).

As can be seen from Figures 4.19 through 4.32, if the pumping is ceased before the level in the immobile region is reduced significantly, the concentrations in the mobile region increase with time. This is not an unexpected result, and has already been observed (22:633) (19).

The creation of this model involved one assumption about diffusion: dispersion $\gg$ diffusion in the mobile region, and therefore diffusion could be ignored. With no pumping there is no guarantee that diffusion in the mobile region will not play an important part in the fate of the pollutant. For this reason, a small pumping rate is maintained, even if it represents a velocity of only a few millimeters per day.

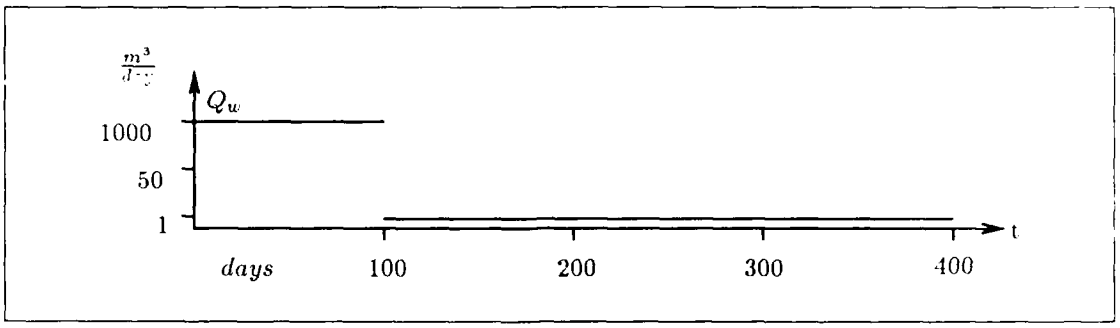

Figure 4.16. Pulse Pumping Schedule for Test 1

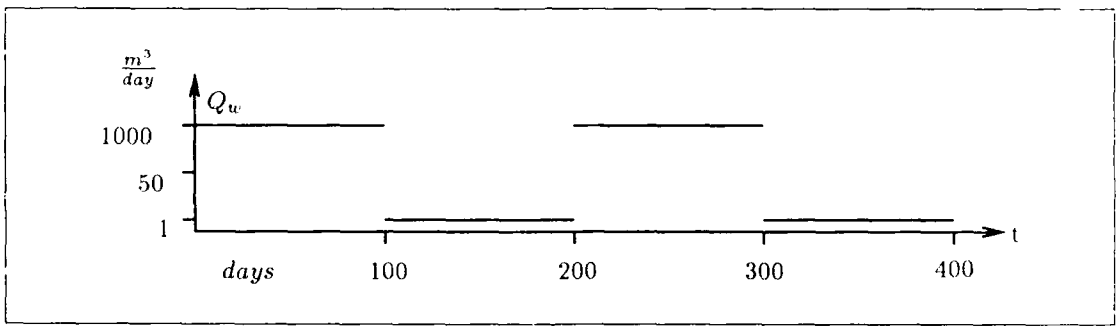

Figure 4.17. Pulse Pumping Schedule for Test 2

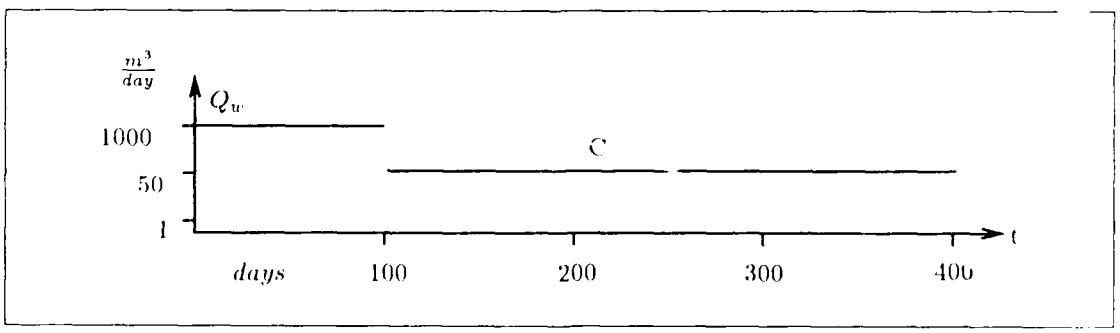

Figure 4.18. Pulse Pumping Schedule for Test 3

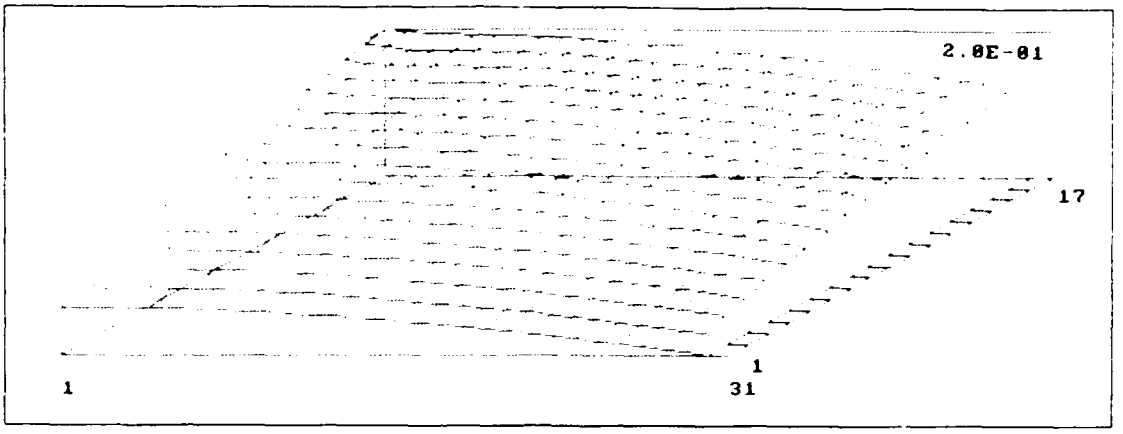

Figure 4.19. Pulse Pumping Test 1; Negligible Flow, Progress from Days 100–200

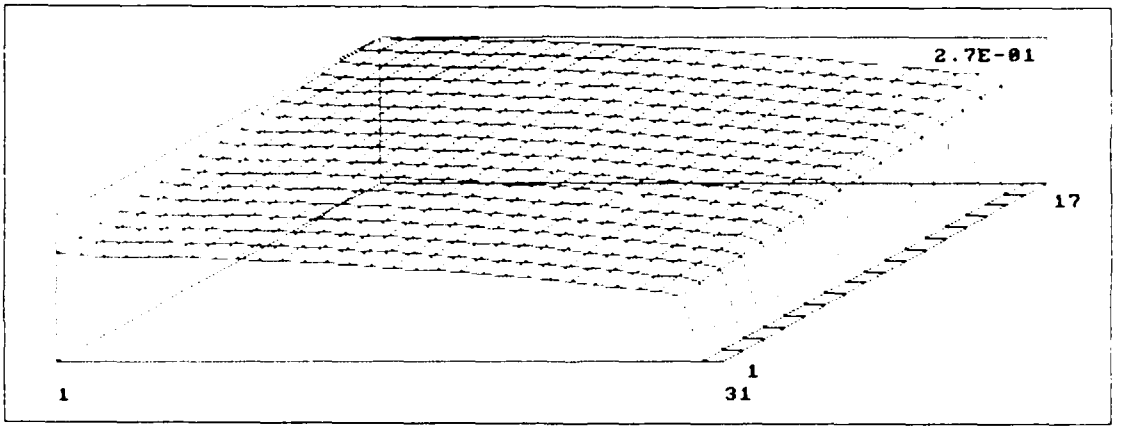

Figure 4.20. Pulse Pumping Test 1; Negligible Flow, Progress from Days 200–300

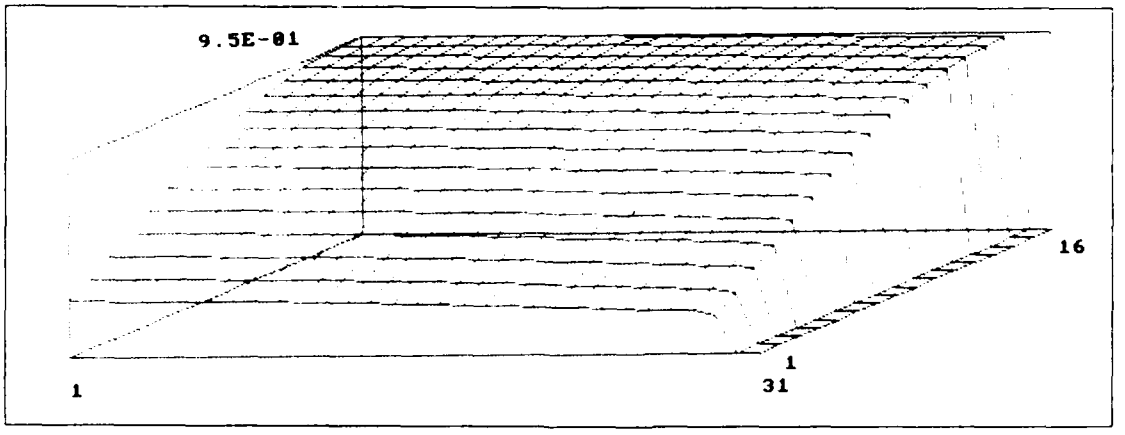

Figure 4.21. Pulse Pumping Test 1; Immobile Region Profile at Day 300

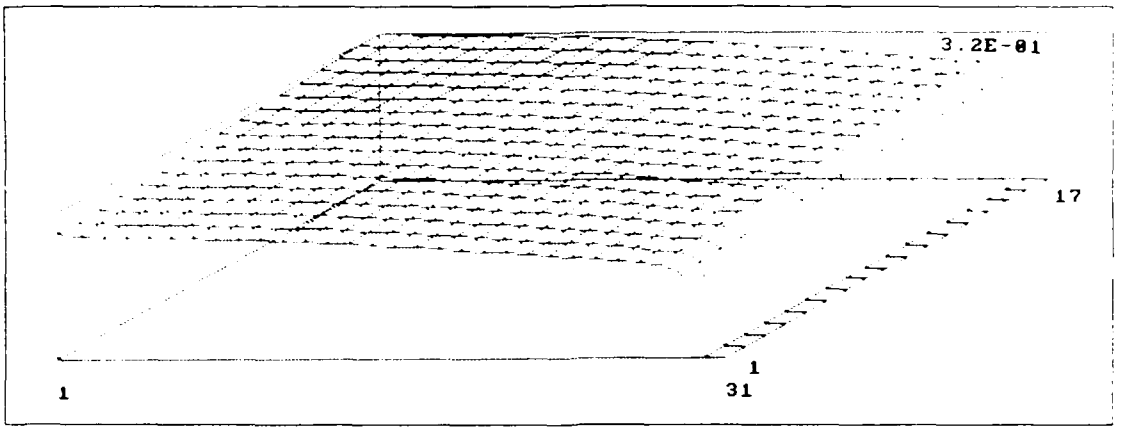

Figure 4.22. Pulse Pumping Test 1; Negligible Flow, Progress from Days 300–400

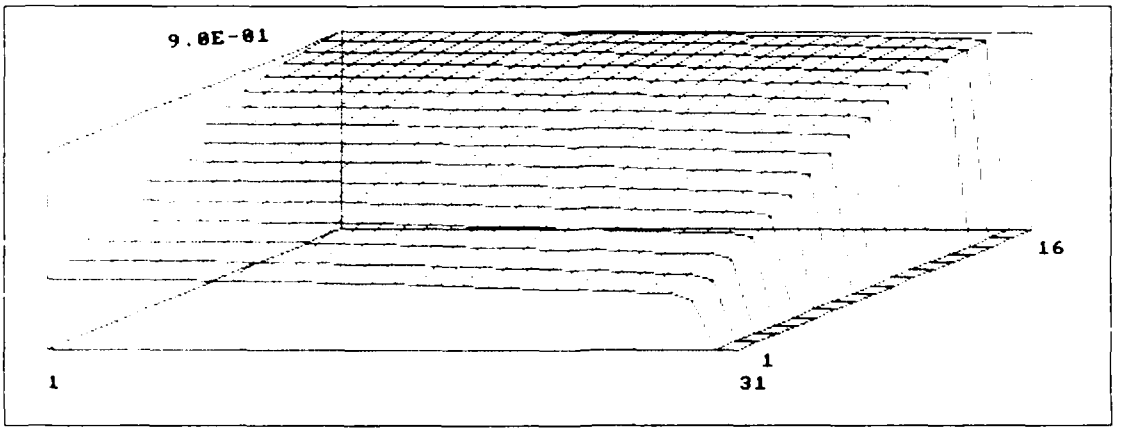

Figure 4.23. Pulse Pumping Test 1; Immobile Region Profile at Day 400

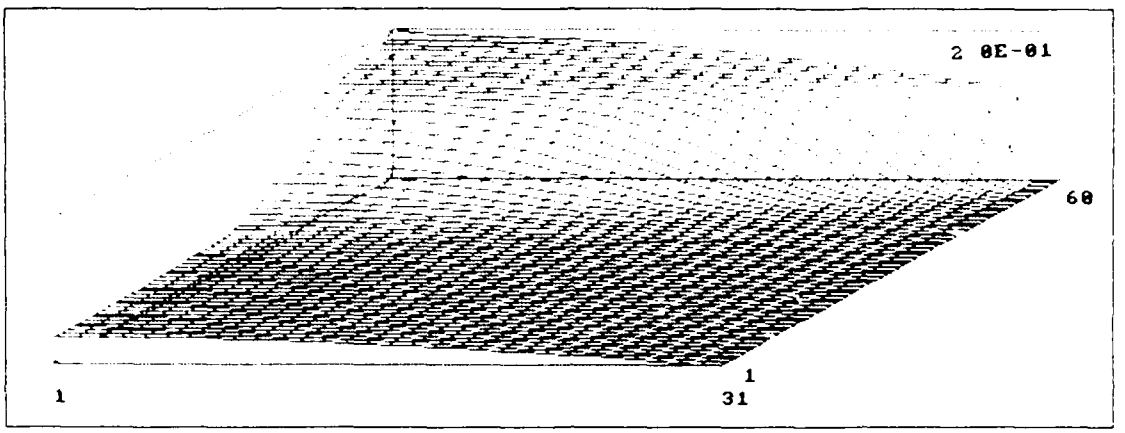

Figure 4.24. Pulse Pumping Test 2; Normal Flow, Progress from Days 200–300, (reversed perspective)

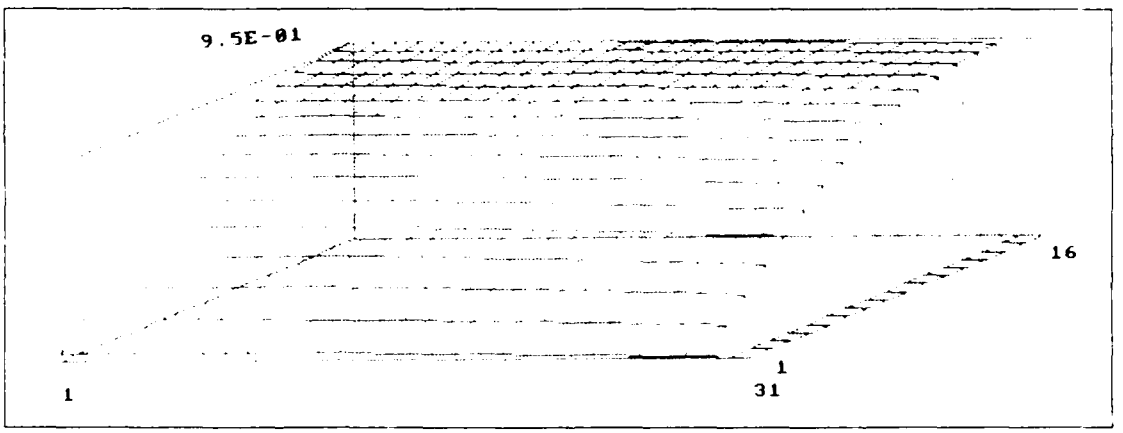

Figure 4.25. Pulse Pumping Test 2; Immobile Region Profile at Day 300

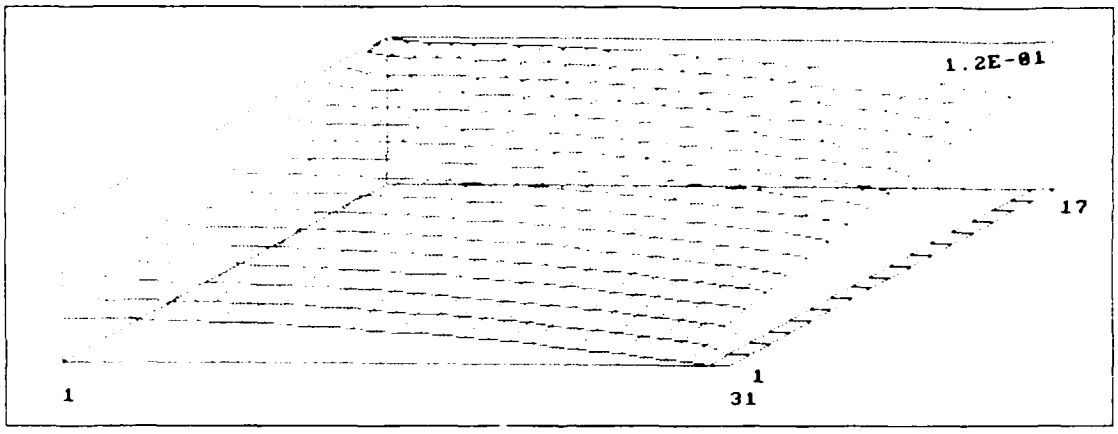

Figure 4.26. Pulse Pumping Test 2; Negligible Flow, Progress from Days 300–400

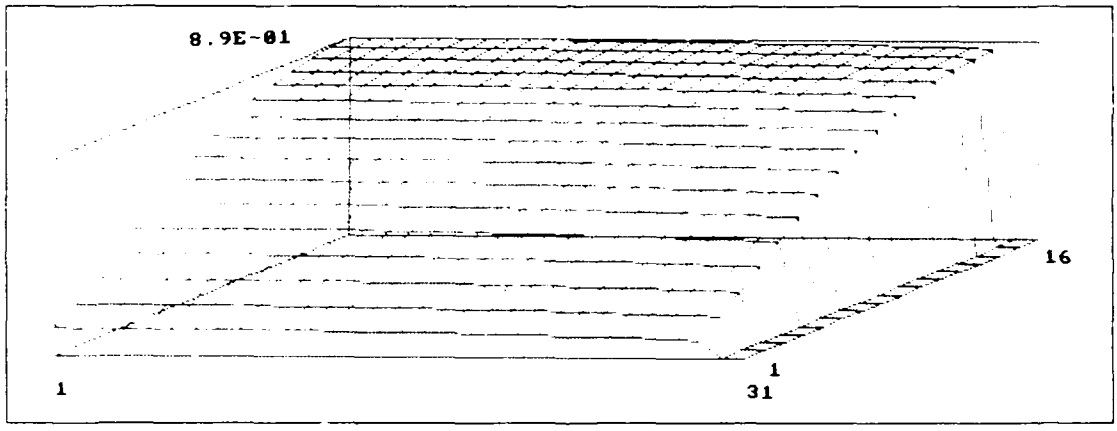

Figure 4.27. Pulse Pumping Test 2; Immobile Region Profile at Day 400

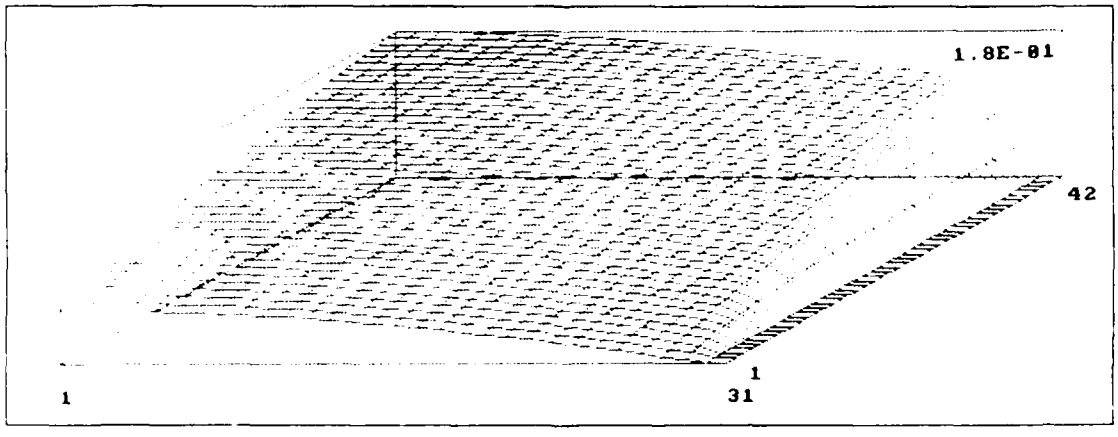

Figure 4.28. Pulse Pumping Test 3; Reduced Flow, Progress from Days 100–200

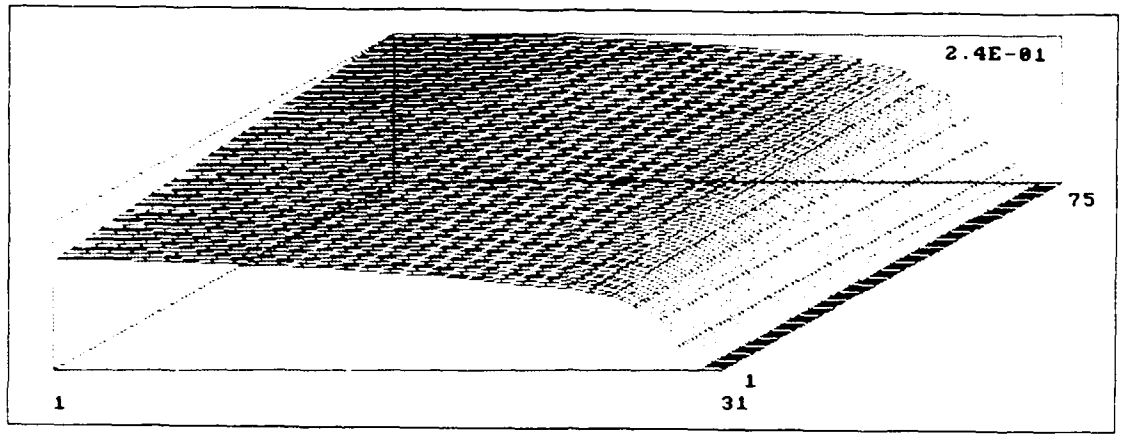

Figure 4.29. Pulse Pumping Test 3; Reduced Flow, Progress from Days 200–300

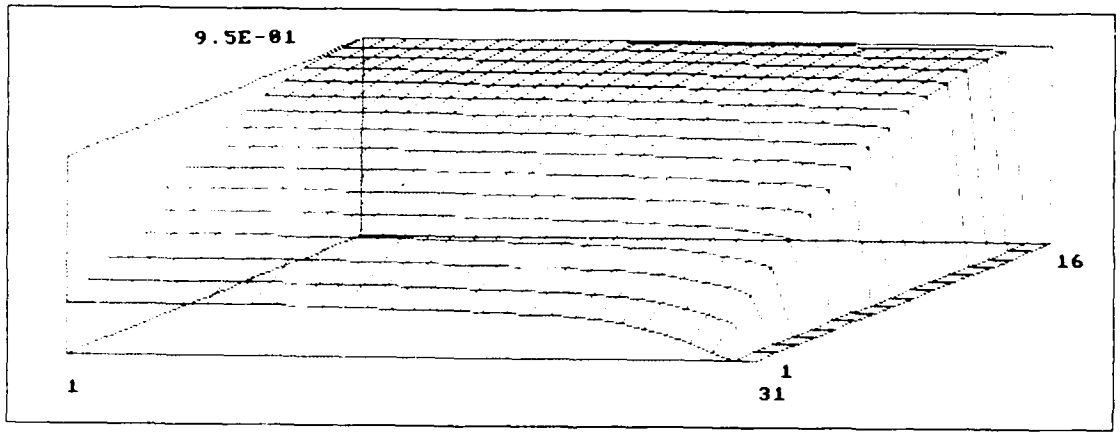

Figure 4.30. Pulse Pumping Test 3; Reduced Flow, Immobile Region Profile at Day 300

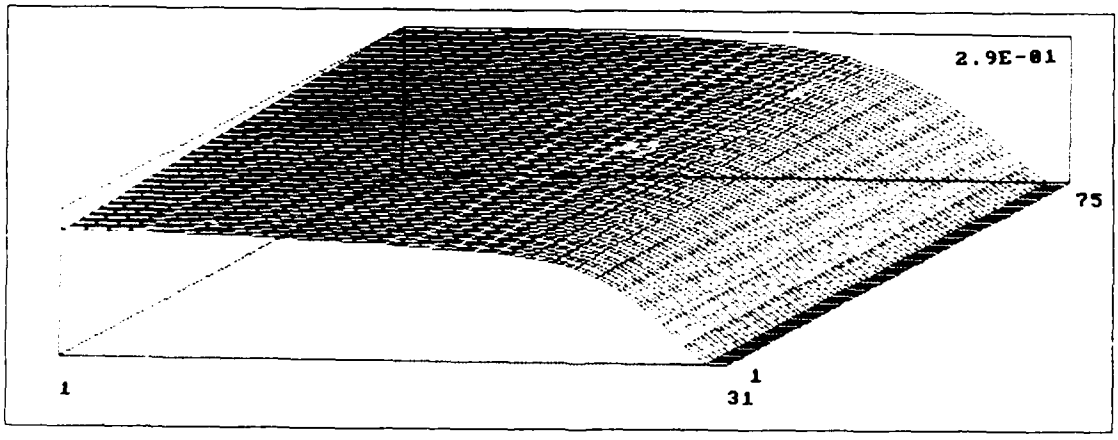

Figure 4.31. Pulse Pumping Test 3; Reduced Flow, Progress from Days 300–400

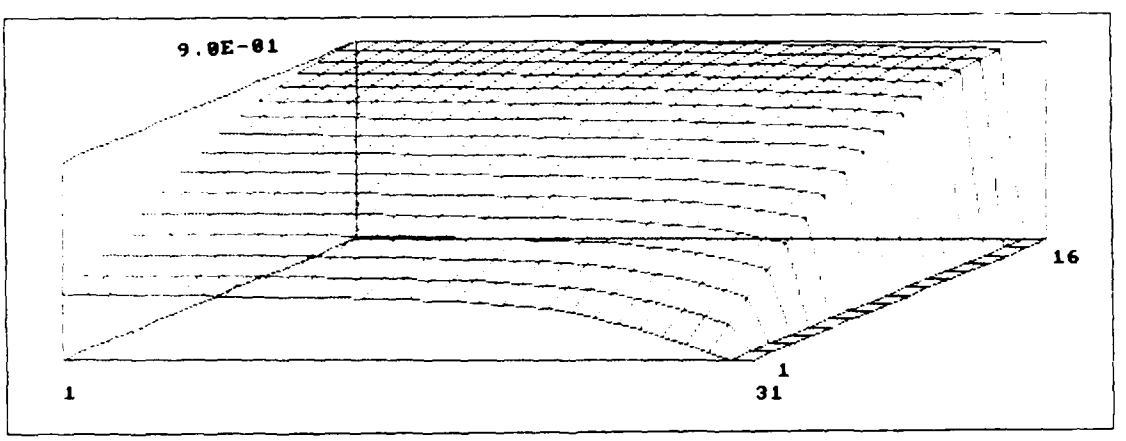

Figure 4.32. Pulse Pumping Test 3; Reduced Flow, Immobile Region Profile at Day 400

V. *Conclusions and Recommendations*

This concluding chapter draws together the research presented in the previous chapters. It focuses on how the research may improve the ability of planners to estimate the needed duration time of remediation pumping. It also shows how slow sorption and desorption of chemicals in porous media could play an important part in the fate of pollutants. Secondly, it enumerates the conclusions which may be drawn from the research. Finally, it lists recommendations both for improvements and for the follow-on efforts to this research.

5.1 Summary

The literature survey revealed that research in the last few decades has contributed to an improved understanding of the desorption processes in contaminant transfer through porous media. Although there's been an increase in our abilities to mathematically model this contaminant transport, there exists a paucity of computer based solutions that incorporate rate-limited desorption.

5.2 Conclusions

Several conclusions could be drawn from the comparison of this computer based solution to the contaminant transport equations with the analytical solution provided by Goltz. Unfortunately, without a large database for comparison with field data or laboratory experiment, we can not properly evaluate this research. An initial laboratory experiment will be conducted shortly by Dr. Burris (7), but not soon enough to add to this thesis. That laboratory experiment will consist of monitoring the contaminant levels in a three dimensional physical model with axial symmetry. A four foot diameter tank will be filled with a sand or soil material, and will have a fully penetrating well in the center of the tank. The contaminant concentrations at the well and in the tank will be monitored.

If the laboratory experiments yield favorable comparisons with this numerical solution, and display similar tailing of contaminants, this simple model could be distributed to planners at toxic cleanup sites for incorporation into their computer toolkit.

5.3 Recommendations

Most of the drawbacks of this model stem from the assumptions made in the *Assumptions* section of Chapter 1. The primary emphasis for future research is to eliminate these assumptions (in the order given):

1. Eliminate the necessity for spherical symmetry; make the mathematical model truly two-dimensional.
2. Add the ability to simulate multiple wells, including injection wells.
3. Create a user-friendly input port for the contaminant profile; probably based on mouse-driven inputs on an Amiga or a Sun workstation.
4. Add the ability to estimate the total contaminant remaining in the aquifer, and the rate at which it will desorb at normal seepage rates.

Other improvements could include correcting the problem with the apparent radius when using diffusion into spherical aggregates. Only experimentation will indicate if this is advised. Also, instead of allowing only spherical or layered immobile material, allow the third possibility: cylindrical immobile material. One additional enhancement could be a further simplification of the existing code to use the first-order models presented by Coats and Smith (10), van Genuchten (36), and Valocchi (33).

5.4 Remarks

As industrial development continues, and as long as Murphy's laws apply, there will be unfortunate instances of polluted groundwater to address. This, together with the need to cleanup the existing toxic spill sites, make this an important piece of research for the environmentally conscious community. This research has endeavored to further the cause of numerical modeling applied to porous media, and to provide the community with another tool to help in the field.

Appendix A. *Notation*

These are most of the variables or constants used in this Thesis. Parenthesized names are the variable names used in MODEL1T representing the same data.

A_l — $[L]$ Dispersivity in the mobile region (alphaL)

b — $[L]$ Characteristic length of the immobile region geometry, the halfwidth or radius of the immobile region

C — $[M/L^3]$ Concentration of adsorbate in the fluid stream: Solute concentration

C_m — $[M/L^3]$ Solute concentration vector in the mobile region (Cm)

C_{im} — $[M/L^3]$ *Solute concentration vector in the immobile region (Cim)*

C_{ima} — $[M/L^3]$ Volume averaged solute concentration vector for the immobile region (Cima)

D — $[L^2/T]$ Hydrodynamic dispersion coefficient

D_e — $[L^2/T]$ Diffusion coefficient within the immobile region (De)

D^* — $[L^2/T]$ Diffusion coefficient within the mobile region

f — [unitless] Fraction of sorption sites in direct contact with mobile water (ef)

H — $[L]$ Average height of the aquifer

K — $[T^{-1}]$ *Exchange rate between stagnant and mobile water*

K_d — $[L^3/M]$ Distribution Coefficient (Kd)

Q_w — $[L^3/T]$ Flow rate at the well (Flow), extraction being positive

r — $[L]$ Radial coordinate within the mobile region; $0 \leq r \leq R$

R — [unitless] Average retardation factor: $R = 1 + \frac{\rho K_d}{\theta}$ (retardation is a friction-type force that slows the progress of the contaminant relative to the flow of groundwater velocity, typical values are 1...33): also used as the maximum extent of the contaminated aquifer in the radial dimension $[L]$

R_m — [unitless] Mobile region retardation factor: $R_m = 1 + \frac{f\,\rho\,K_d}{\theta_m}$ (Rm)

R_{im} — [unitless] Immobile region retardation factor: $R_{im} = 1 + \frac{(1-f)\,\rho\,K_d}{\theta_{im}}$ (Rim)

S — $[M/L^3]$ Sorbed solute concentration, or [unitless] sorbed contaminant

t — $[T]$ Time

$V(r)$ — $[L/T]$ Velocity of the groundwater through the interstices of the aquifer (mobile regions only)

— Greek —

α $[T]$ Basis function (temporal extent)

z $[L]$ Spatial coordinate within the immobile region

β [unitless] Solute capacity ratio of the immobile to mobile regions: $\beta = \frac{\theta_{im} R_{im}}{\theta_m R_m}$ (beta)

θ — [unitless] Porosity or Total water content: $\theta = \theta_m + \theta_{im}$ (theta), also called total porosity (typical values for granular aquifers are 20–40%)

θ_{im} — [unitless] Immobile water content, also called immobile region porosity

θ_m — [unitless] Mobile water content (thetaM), also called mobile region porosity

λ — [unitless] Fraction representation of stagnant to mobile water

π — [unitless] Ratio of diameter of a circle to its circumference

ρ — $[M/L^3]$ Bulk density of aquifer material (rho): rho is also used as a constant in the model

τ — [unitless] Integration variable

ϕ — $[L]$ Basis functions (spatial extent), also [unitless] ratio of mobile to total water content: $\phi = \theta_m/\theta$ (phi)

Bibliography

1. Absoft Corporation:, 2781 Bond St, Auburn Hills, MI 48057. *AC/FORTRAN, ANSI FORTRAN 77 Compiler with Debugger* (2.3 Edition), 1989.

2. Bear, Jacob. *Dynamics of Fluids in Porous Media*. American Elsevier Publishing Company, Inc., 1972.

3. Bear, Jacob and Arnold Verruijt. *Modeling Groundwater Flow and Pollution*. P.O. Box 17, 3300 AA Dordrecht, Holland: D. Reidel Publishing Company, 1987.

4. Blake, William. *The Complete Poems*. Harmondsworth, Middlesex, England: Penguin Books, Ltd., 1977.

5. Bouchard, D. C., et al. "Sorption Nonequilibrium During Solute Transport," *Journal of Contaminant Hydrology*, pages 209–223 (1988).

6. Brusseau, Mark L. and P. S. C. Rao. "Sorption Nonideality During Organic Contaminant Transport in Porous Media," *Critical Reviews in Environmental Control*, *19*(1):33–99 (1989).

7. Burris, David R., September 1989. Personal Communication and Correspondence with Dr. David R. Burris, Research Chemist, HQ Air Force Engineering and Services Center.

8. Burris, David R., et al. "Organic Chemical Sorption Kinetic Effects Measured on Columns of Humic Acid Coated Silica." Submitted to Environmental Science and Technology, June 1989.

9. Chen, Chia-Shyun and Greg D. Woodside. "Analytical Solution for Aquifer Decontamination by Pumping," *Water Resources Research*, *24*(8):1329–1338 (August 1988).

10. Coats, K. H. and B. D. Smith. "Dead-End Pore Volume and Dispersion in Porous Media," *Society of Petroleum Engineers Journal*, pages 73–84 (March 1964).

11. Crittenden, John C., et al. "Transport of Organic Compounds With Saturated Groundwater Flow: Model Development and Parameter Sensitivity," *Water Resources Research*, *22*(3):271–284 (March 1986).

12. Foreman, Dave and Bill Haywood, editors. *Ecodefense: A Field Guide to Monkeywrenching* (second Edition). P.O. Box 5871, Tucson, AZ 85703: Ned Ludd Books, 1987.

13. Goltz, Mark N., "Modeling the Effect of Rate-Limited Desorption of Organic Contaminants Upon Aquifer Decontamination," December 1988. AUG Fall Meeting.

14. Goltz, Mark N. "Contaminant Transport Modeling and the Installation Restoration Program." Accepted for Publication by *The Military Engineer*, February 1989.

15. Goltz, Mark N. *Three-Dimensional Analytical Modeling of Diffusion-Limited Solute Transport*. PhD dissertation, Stanford University, July 1986.

16. Goltz, Mark N. and Paul V. Roberts. "Simulations of Physical Nonequilibrium Solute Transport Models: Application to a Large-Scale Field Experiment," *Journal of Contaminant Hydrology*, pages 37–63 (1988).

17. Haltiner, George J. and Roger Terry Williams. *Numerical Prediction and Dynamic Meteorology*. John Wiley & Sons, Inc., 1980.

18. Illangasekare, Tissa H. and Petra Döll. "A Discrete Kernel Method of Characteristics Model of Solute Transport in Water Table Aquifers," *Water Resources Research*, *25*(5):857–867 (May 1989).

19. Keely, J. F., et al. "Optimizing Recovery of Contaminant Residuals By Pulsed Operation of Hydraulically Dependent Remediations." In *Proceedings of the NWWA/API Conference on Petroleum Hydrocarbons and Organic Chemicals in Ground Water—Prevention, Detection, and Restoration*, pages 91–103, 6375 Riverside Dr. Dublin, OH 43017: National Water Well Association, November 1987.

20. Lapidus, Leon and Neal R. Amundson. "Mathematics of Adsorption in Beds.," *Journal of Physical Chemistry*, *56*(8):984–988 (November 1952).

21. Leismann, H. M., et al. "A Quick Algorithm for the Dead-End Pore Concept for Modeling Large-Scale Propagation Processes in Groundwater." In *Vol.2 Numerical Methods for Transport and Hydrologic Processes*, pages 275–280, June 1988.

22. Mackay, Douglas M. and John A. Cherry. "Groundwater Contamination: Pump-and-treat Remediation," *Environmental Science and Technology*, *23*(6):630–636 (1989).

23. Meissner, Loren P. and Elliot I. Organick. *Fortran 77*. Addison-Wesley Publishing Company, 1980.

24. Miller, Cass T. and Walter J. Weber, Jr. "Sorption of Hydrophobic Organic Pollutants in Saturated Soil Systems," *Journal of Contaminant Hydrology*, pages 243–261 (1986).

25. Nkedi-Kizza, R., et al. "Ion Exchange and Diffusive Mass Transfer During Miscible Displacement Through an Aggregated Oxisol," *Soil Science Society of America Journal*, *46*:471–476 (1982).

26. P., Gamerdinger A. and P. S. C. Rao, "An Evaluation of the Use if In Situ Testing Devices for the Study of Sorption During Transport," September 1989. Presented Before the Division of Environmental Chemistry, American Chemical Society.

27. Press, William H, et al. *Numerical Recipes*. Cambridge University Press, 1986.

28. Pressman, Roger S. *Software Engineering: A Practitioner's Approach* (Second Edition). New York: McGraw-Hill Book Company, 1987.

29. Rao, P. S. C., et al. "Experimental and Mathematical Description of Nonadsorbed Solute Transfer by Diffusion in Spherical Aggregates," *Soil Science Society of America Journal*, *44*(4):684–688 (1980).

30. Southworth, George R., et al. "Comparison of Models that Describe the Transport of Organic Compounds in Macroporous Soil," *Environmental Toxicology and Chemistry*, *6*:251–257 (1987).

31. Strang, Gilbert and George J. Fix. *An Analysis of the Finite Element Method*. Series in Automatic Computation, Prentice-Hall, 1973.

32. Sudickey, E. A., et al. "Experimental Investigation of Solute Transport in Stratified Porous Media 1. The Nonreactive Case," *Water Resources Research*, *21*(7):1035–1041 (July 1985).

33. Valocchi, Albert J. "Effect of Radial Flow on Deviations From Local Equilibrium During Sorbing Solute Transport Through Homogeneous Soils," *Water Resources Research*, *22*(12):1693–1701 (November 1986).

34. van der Heijde, Paul K. M., et al. *Groundwater Modeling: An Overview and Status Report*. Technical Report GWMI 88-10, Butler University, Indianapolis, IN 46208: Holcomb Research Institute, December 1988.

35. van Genuchten, M. Th. and R. W. Cleary. *Soil Chemistry. B. Physico-Chemical Models*, chapter Movement of Solute in Soil: Computer-simulated and Laboratory Results, pages 349–386. Elsevier Scientific Publishing Co., 1982.

36. van Genuchten, M. Th. and P. J. Wierenga. "Mass Transfer Studies in Sorbing Porous Media 1. Analytical Solutions," *Soil Science Society of America Journal*, *40*(4):473–480 (1976).

37. Wu, Shian-Chee and Philip M. Gschwend. "Numerical Modeling of Sorption Kinetics of Organic Compounds to Soil and Sediment Particles," *Water Resources Research*, *24*(8):1373–1383 (August 1988).

38. Young, David M. and Robert Todd Gregory. *A Survey of Numerical Mathematics*. Dover Publications, Inc., 1988.

Vita

Captain Rand C. Huso was born on 21 June 1955 in Fairmont, Minnesota. In 1973 he graduated from Auburn High School, Auburn, Washington, and then attended two years of college before being expelled for low grades. In 1975 he joined the Air Force and worked as a firefighter for 5 years. Then in December of 1982 he graduated from Pacific Lutheran University in Tacoma, Washington, with a Bachelor of Science degree in Engineering-Physics and a Minor in Mathematics. Captain Huso joined the Air Force again in 1983 and received his commission from the Officer Training School in San Antonio, Texas. Then he attended Texas A&M University in College Station, Texas, for one year and received an equivalent Bachelor degree in Meteorology. He served as a Numerical Analyst for Air Force Global Weather Central at Offutt Air Force Base in Omaha, Nebraska, and then as a Wing Weather Officer at Comiso A.S., Italy, before entering the School of Engineering, Air Force Institute of Technology, in May, 1988.

Permanent address: 25810 SE 392d Avenue
Enumclaw, Wa 98022

Abstract

This paper traces the development of the understanding of contaminant transport in an aquifer for a radially symmetric region. It presents the progression of ideas and equations leading to the equation set describing the advective/dispersive mechanisms coupled with rate-limited adsorption. This equation set is converted to a numerical scheme in the Fortran language using finite elements and finite differences. The resulting model is tested against the Laplace transform solution to the same equation set, and several graphs are presented detailing the comparison.

UNCLASSIFIED

SECURITY CLASSIFICATION OF THIS PAGE

REPORT DOCUMENTATION PAGE

Form Approved OMB No. 0704-0188

1a. REPORT SECURITY CLASSIFICATION UNCLASSIFIED	1b. RESTRICTIVE MARKINGS
2a. SECURITY CLASSIFICATION AUTHORITY	3. DISTRIBUTION / AVAILABILITY OF REPORT Approved for public release, Distribution unlimited
2b. DECLASSIFICATION / DOWNGRADING SCHEDULE	
4. PERFORMING ORGANIZATION REPORT NUMBER(S) AFIT/GCS/ENC/89D-2	5. MONITORING ORGANIZATION REPORT NUMBER(S)
6a. NAME OF PERFORMING ORGANIZATION School of Engineering 6b. OFFICE SYMBOL (If applicable) AFIT/ENC	7a. NAME OF MONITORING ORGANIZATION
6c. ADDRESS (City, State, and ZIP Code) Air Force Institute of Technology WPAFB, OH 45433-6583	7b. ADDRESS (City, State, and ZIP Code)
8a. NAME OF FUNDING / SPONSORING ORGANIZATION Air Force Institute of Tech 8b. OFFICE SYMBOL (If applicable) AFIT/ENC	9. PROCUREMENT INSTRUMENT IDENTIFICATION NUMBER
8c. ADDRESS (City, State, and ZIP Code) Air Force Institute of Technology WPAFB, OH 45433-6583	10. SOURCE OF FUNDING NUMBERS PROGRAM ELEMENT NO. / PROJECT NO. / TASK NO / WORK UNIT ACCESSION NO

11. TITLE (Include Security Classification)

NUMERICAL MODELING OF CONTAMINANT TRANSPORT WITH RATE LIMITED SORPTION/ DESORPTION IN AN AQUIFER

12. PERSONAL AUTHOR(S)

Huso, Rand Cary, Capt, USAF

13a. TYPE OF REPORT	13b. TIME COVERED	14. DATE OF REPORT (Year, Month, Day)	15. PAGE COUNT
MS Thesis	FROM _____ TO _____	December 1989	65

16. SUPPLEMENTARY NOTATION

17. COSATI CODES			18. SUBJECT TERMS (Continue on reverse if necessary and identify by block number)
FIELD	GROUP	SUB-GROUP	
23	01		Rate-Limited Adsorption, Contaminant Transport
12	01		

19. ABSTRACT (Continue on reverse if necessary and identify by block number)

THESIS CHAIRMAN: Dr. Mark Oxley
Associate Professor of Mathematics

ABSTRACT: (See reverse)

20. DISTRIBUTION / AVAILABILITY OF ABSTRACT ☒ UNCLASSIFIED/UNLIMITED ☐ SAME AS RPT ☐ DTIC USERS	21. ABSTRACT SECURITY CLASSIFICATION UNCLASSIFIED
22a. NAME OF RESPONSIBLE INDIVIDUAL Dr Mark Oxley	22b. TELEPHONE (Include Area Code) 513-255-3098 22c. OFFICE SYMBOL AFIT/ENC

DD Form 1473, JUN 86 *Previous editions are obsolete.*

SECURITY CLASSIFICATION OF THIS PAGE

UNCLASSIFIED

END

FILMED

1-90

DTIC